TEMPORAL AND SPATIAL GROWTH OF SUBHARMONIC DISTURBANCES IN FALKNER-SKAN FLOWS

by

Fabio P. Bertolotti

Thesis submitted to the Graduate Faculty of the Virginia Polytechnic Institute and State University in partial fulfillment of the requirements for the degree of

MASTER OF SCIENCE
in
Engineering Mechanics

Approved:

Dr. T. Herbert, Chairman

Dr. A. H. Nayfeh

Dr. D. T. Mook

June 1985
Blacksburg, Virginia

ACKNOWLEDGEMENTS

Foremost in the author's list of gratitude is Dr. T. Herbert, whose ideas form the supporting structure for this thesis, and whose concise and clear explanations have guided and stimulated the author through the intricate field of hydrodynamic stability. Thanks are given also to Dr. A.H. Nayfeh and Dr. D.T. Mook for their participation and contribution as committee members.

In the computational end of the work, special thanks are given to Dr. Thompson and C. Hawley for their kind help. Gratitude is also extended to fellow researchers, doctor R. Li, G. Santos, and J. Croswell for helpful discussions.

This work was supported by the Office of Naval Research under Contracts N0014-83-K-0089 and N0014-84-K-0093.

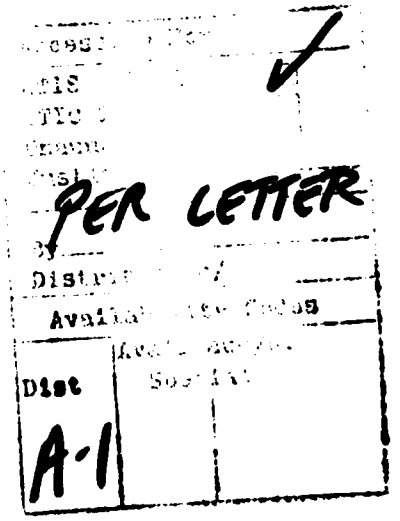

TABLE OF CONTENTS

INTRODUCTION

1. Scope of the thesis

Careful experiments on boundary layer transition conducted in low turbulence wind tunnels have resolved three stages in the breakdown of laminar flow into turbulence: in the first stage, two-dimensional oscillations, commonly referred to as TS waves, appear and propagate in the direction of the flow; in the second stage there appears a rapid three-dimensional deformation of the oscillatory flow; and in the brief third stage high frequency, small scale, quasi-random fluctuations appear and quickly lead the flow into turbulence.

The recent analysis of the second stage based on a secondary instability mechanism arising from a parametric resonance induced by the TS wave has given results in quantitative agreement with experimental observations. Using this approach, Herbert has studied the phenomenon in plane channel flow and in a Blasius boundary layer [1-5]. The present work studies the effect of pressure gradients on the behavior of secondary instabilities. by extending Herbert's analysis to the Falkner-Skan family of profiles, and develops a spatial formulation for disturbance growth to exactly match the experimentally observed behavior.

2. Motivation

The study of secondary instabilities in the Falkner-Skan family of profiles, and hence in flows with pressure gradients, is a necessary step towards the analysis of transition on objects with a non-constant surface pressure distribution, foremost among which are airfoils. In high-Reynolds-number aerodynamics the effect of transition is mainly a quantitative change in drag. At low Reynolds number, and in combination with a separating boundary layer in strong adverse pressure gradients, the location of transition and the structure of the transitional flow can affect the global flow field about the airfoil. Indeed, with the presence of the second stage of transition in a boundary layer undergoing separation, the three-dimensional disturbances can activate strong vortex stretching in the subsequent free shear layer and cause breakdown into wall bound turbulence, forming a separation bubble, while the absence of three dimensionality at separation can allow periodical vortex pairing in the free shear layer and postpone turbulence far enough downstream to cause the layer to permanently leave the surface, creating a condition of stall over the airfoil. A visual representation of this idea is given in figure 1. Hence in both high and low Reynolds number external flows the presence and structure of transition is an important phenomenon.

In the past eight decades, starting with the work of Orr and Sommerfeld, extensive study has been done on the first stage (primary instabilities) using the method of small oscillations. This approach yields correctly the downstream location (critical Reynolds number) at which instability initiates, and describes accurately the oscillatory field at small amplitudes.

However, it cannot model the evolution of the three-dimensional stage, and, when used in conjunction with a e^n transition criterion, it gives transitional predictions erroneously independent of the upstream background disturbance amplitudes.

The secondary instability model used in the present work overcomes these shortcomings by incorporating the background disturbance amplitudes as a parameter, and predicting in agreement with observation the form and growth rate of secondary disturbances. We should mention, however, that this model is not complete in itself, for it does not include a criterion for determining the conditions at which the three-dimensional disturbances develop a "life of their own" by becoming independent from the parametric excitation of the TS wave as a source of growth. This step, along with the usage of actual airfoil boundary layer profiles in a downstream marching transition prediction analysis, will be a future extension of the present work.

3. Experimental view of boundary layer transition

In the study of boundary layer transition the majority of the experimental results have been obtained by using the vibrating ribbon technique of Schubauer & Skramstad [6], in which the transition over a body immersed in a low turbulence stream is initiated, and hence, controlled by the regulated vibration of a tightly stretched ribbon. A more detailed account of the following descriptions can be found in Klebanoff, Tidstrom, & Sargent [7], Kachanov & Levchenko [8] , or in Saric et al. [9]. Let the streamwise, normal-to-plate, and spanwise directions compose an orthogonal system. In a low noise environment a streakline observation in a boundary layer con-

taining a forced oscillation, introduced by a vibrating ribbon, might proceed as follows:

- At low oscillation amplitudes one observes traveling waves (TS waves) invariant in the spanwise direction and propagating with the the flow. Their amplitude harmlessly grows and decays in full accordance with linear stability theory. Turbulence is delayed to high Renoylds numbers.

- When the amplitude of the TS wave is increased and a certain critical combination of Reynolds number and amplitude is reached, the wave experiences a rapid spanwise periodic deformation. One can observe spanwise alternating peaks and valleys which indicate the presence of enhanced and reduced wave amplitude. The peak-valley structure is staggered, repeating itself with twice the periodicity of the TS wave (see Fig. 2a), and fixed hot wire measurements record subharmonic signals. The rapid growth of the three-dimensional structure leads to the formation of concentrated shear layers at the peak positions. The highly inflectional velocity distribution quickly breaks up into tertiary instabilities.

- At higher initial levels of the TS amplitude the above phenomenon is repeated, but with a different structure; the peaks and valleys are aligned, repeating themselves with the same frequency and periodicity as the TS wave. A system of streamwise vortices appears simultaneously with the aligned peaks and valleys (see Fig. 2b). Being first observed in 1962 by Klebanoff et al. it is usual today to name this

aligned peak-valley splitting as K-type breakdown. The disturbances undergo pure spatial growth in all the above cases.

4. Review of past research

The three stages of boundary layer transition described have also been observed in plane Poiseuille flow [10], in free shear layers [11], and in a fluid with continuously stratified density (internal gravity waves) [12]. In all three flows, researchers have tried to model the second stage of transition using two approaches: weakly nonlinear models, or parametric instability models. The latter one has given the most general and accurate results.

Weakly nonlinear models appeared following the innovative work of Landau. As discussed by Drazin and Reid [13], one can expand the velocity field in weakly nonlinear analysis as

$$\mathbf{v} = \sum_{i=1}^{\infty} A_i(t)\mathbf{f}_i(\mathbf{x}) \; + \; \textit{Complex Conj.} \qquad (1)$$

where $\{ \mathbf{f}_i \}$ is a complete set of functions satisfying the boundary conditions, and is usually taken to be the wave type modes of the linear problem (Orr-Sommerfeld or Squire modes in boundary layers, Helmholtz modes in free shear layers). When the series is inserted into the Navier-Stokes equation the nonlinear convective term $(\mathbf{v}\cdot\nabla)\mathbf{v}$ creates resonant wave interactions. The interaction is, by computational necessity, limited to a finite number of waves by truncating the series to a few terms, usually three. Different weakly nonlinear models stem from different selections of modes in the truncated series. For compactness we introduce the wave vector $\mathbf{k} = (\alpha,\beta)$, where α is the streamwise wavenumber and β is the

(perpendicular) spanwise wave number.

The model of Benney and Lin [14], 1960, attempts to describe the Klebanoff type structure by considering the interaction between the TS wave, $\mathbf{k}_o = (\alpha,0)$, and two oblique modes of the Orr-Sommerfeld equation (OSE), $\mathbf{k}_1 = (\alpha, +\beta)$ and $\mathbf{k}_2 = (\alpha, -\beta)$, with β as a free parameter. Whether or not conditions for phase synchronization of the three modes exist is still a subject of debate [15]. The model due to Craik [16] uses the TS wave and two oblique modes of the OSE, $\mathbf{k}_1 = (\alpha/2, +\beta^*)$ and $\mathbf{k}_2 = (\alpha/2, -\beta^*)$ to model the subharmonic structure. The value of β^* is chosen such that the modes $\mathbf{k}_1$ and $\mathbf{k}_2$ have the same phase speed as the TS wave, thus allowing for efficient energy transfer among the three modes. In boundary layers, this model sometimes predicts correctly the value spanwise undulation β, but at other times, under similar experimental conditions, β^* differs widely from the observed value. In plane Poiseuille flow the model is inoperative for reasons of symmetry [17]. Herbert and Morkovin [17] forwarded a model composed of the TS wave and two longitudinal vortices of the OSE equation, $\mathbf{k}_1 = (0, +\beta)$ and $\mathbf{k}_2 = (0, -\beta)$, to model a spanwise periodic longitudinal vortex structure.

Other models have been developed, and the above list is by no means exhaustive. However, along with the weakly nonlinear model the author should present a guarantee of "completeness" of the model, i.e. show that the modes considered are responsible for the observed phenomena. This task is difficult, it is rarely performed, and is the single greatest drawback of the method.

The secondary instability model based on parametric resonance is

intuitively simple to understand using physical arguments. In the first stage of transition the presence of the primary wave brings about a redistribution of vorticity in the flow. When moving with the velocity of the wave, an observer sees a periodically spaced, coplanar arrangement of vortex tubes, sometimes referred to as a "cat's eyes" vorticity pattern. This arrangement is highly unstable to small three-dimensional disturbances: a vortex tube slightly distorted along its length is alternatively placed into regions of faster and slower moving fluid and undergoes rapid stretching. Furthermore, if there is sufficient room, the arrangement is also unstable to small two-dimensional disturbances which tend to amalgamate neighboring vortices into a larger vortex (vortex pairing). The mathematical analysis, hence, can be divided into two parts; the construction of the the periodic flow arising from the first stage of transition, and the analysis of a superimposed three-dimensional velocity perturbation of amplitude sufficiently small for linearization. Due to the spatial periodicity of the basic flow, the instability mechanism is governed by a Floquet system.

The first application of a Floquet system to boundary layer transition seems to have been done by Maseev [18], 1968. However, his work went unobserved, perhaps due to its short presentation and use of an unclear perturbation method for solution. Prior to this work, Floquet theory had been used by Kelly [19], 1967, for the stability study of a inviscid free shear layer. He found the vortex pairing mode to stem from principal parametric (subharmonic) resonance. Pierrehumbert & Widnall [20], 1979, repeated the analysis using a more accurate periodic flow model composed of an array of Stuart vortices.

Observing that certain experimental setups for the study of Lamb-Taylor instabilities excited periodically the flow, Nayfeh [21], 1969, derived a Mathieu type equation to explain the overstability behavior. In the mid and late seventies several researchers applied Floquet theory to model the evolution of three-dimensionality in internal gravity waves. McEwan & Robinson [12], 1975, studied parametric instability driven by time periodic coefficients. Mied [22], 1976, refined the analysis by changing to a frame moving with the periodic wave and solved for temporally growing disturbances, and extended the analysis to Rossby waves [23]. In both studies he shows that "the parametric instabilities reduce to the nonlinear resonant interaction in the limit of vanishing basic state amplitude". Drazin [24], 1977, independently developed a Floquet formulation for this problem, and in his work he related the parametric instability to resonant wave interaction and to the catastrophe theory of Thom. He noted that the Floquet system could be applied to other flows if certain general properties of waves are satisfied.

In 1979, Nayfeh and Bozatli [25] studied the subharmonic vortex pairing in a boundary layer using the method of multiple scales. They showed that a large amplitude of the TS wave (29%) is necessary to initiate the pairing process. This fact is in agreement with the present results. However the analysis was only two-dimensional, while the most unstable subharmonic modes are three-dimensional, with a spanwise wave number of the order of the TS wave.

The application of Floquet theory to the stability study of equilibrium states in plane Poiseuille flow was concurrently developed by Orszag [26]

and Herbert [27], 1981. The former author used the method to verify the linear character of three-dimensional instability as revealed by the disturbances' exponential growth with time in a full numerical simulation of the Navier-Stokes equation. While Orszag focused on large amplitude equilibrium states and subcritical instability, Herbert performed a thorough investigation in the case of small amplitude TS waves, and used the threshold amplitudes, the β selectivity, and other characteristics of secondary instabilities to clarify the experimental observations. He extended the model to the Blasius boundary layer. By a careful study in the limit of vanishing TS wave amplitude he was able to determine some circumstances in which weakly nonlinear models were complete and others in which the models failed to account for the dominant modes [4]. By means of a crude transformation from temporal to spatial growth rates, the experimentally observed streamwise amplitude variation of the subharmonic was astonishingly reproduced by the theory [2], confirming the parametric nature of instability in the second stage of transition.

GOVERNING EQUATIONS FOR SECONDARY INSTABILITY

The following derivation is confined to steady, incompressible, constant temperature shear-layer flows having a weak variation in the streamwise coordinate. In the derivation we follow Herbert [1-5]. The analysis is divided into two parts: the construction of the periodic basic flow and the investigation of superposed secondary disturbances with amplitudes sufficiently small for linearization.

1. Construction of the Periodic Basic Flow

We consider the flow over a semi-infinite plate at an angle $P\pi/2$ to the free stream. Let X denote the distance from the leading edge along the plate, Y the distance normal to the plate, and z the spanwise coordinate, $U_e = kX^{P/(2-P)}$ the inviscid flow velocity at the surface, and X_0 the location at which the stability analysis is performed. The undisturbed boundary layer stream function is given by

$$\Psi_{FS}(X,Y,t) = U_e f(y)\delta \quad , \quad \delta = \left[(2-P)\frac{\nu x}{U_e}\right]^{\frac{1}{2}} \quad , \quad y = \frac{Y}{\delta} \qquad (1)$$

where $f(y)$ satisfies the Falkner-Skan equation

$$f''' + ff'' + P(1-f'^2) = 0 \qquad (2)$$

$$f(0) = f'(0) = 0 \, , \, f'(y-\infty) = 1 \qquad (3)$$

We use δ and U_e as characteristic quantities for nondimensionalization, and define the Reynolds number by $R = U_e\delta/\nu$. At sufficiently high R, primary disturbances appear, and during their initial stages of growth they are well modeled by linear stability analysis. Only a general overview of the analysis will be given here. For a detailed description see ,for example, Betchov and Criminale [28]. We superimpose a small disturbance $\mathbf{v}_1$ on the basic flow $\mathbf{V}$,

$$\mathbf{v}(X,y,z,t) = \mathbf{V}(X,y) + A\,\mathbf{v}_1(X,y,z,t) \tag{4}$$

$$A \ll 1 \tag{5}$$

and insert this compound flow into the Navier-Stokes equation. The nonlinear convective term $A^2(\mathbf{v}_1\cdot\nabla)\,\mathbf{v}_1$ is dropped in view of the small amplitude of the disturbance. Collecting terms of order A one obtains linear governing equations for $\mathbf{v}_1$,

$$\frac{\partial}{\partial t}\mathbf{v}_1 + (\mathbf{v}_1\cdot\nabla)\mathbf{V} + (\mathbf{V}\cdot\nabla)\mathbf{v}_1 = -\nabla p_1 + \frac{1}{R}\nabla^2\mathbf{v}_1 \tag{6}$$

$$\nabla\cdot\mathbf{v}_1 = 0 \tag{7}$$

subject to the boundary conditions $\mathbf{v}_1(X,0,z,t) = 0$, $\mathbf{v}_1(X,\ y\to\infty\ ,z,t) = 0$. Equation (6) is separable in t and z. Due to the weak variation of the Falkner-Skan profile with X, we apply the parallel-flow approximation and assume the profile to be locally one-dimensional, $\mathbf{V}_o(X_o,y)$. Then the disturbance equation becomes separable also in X, and the solution can be expressed with normal modes in the variables X , t , and z. The error associated with the parallel-flow approximation is small in profiles with favorable pressure gradients, $P \geq 0$, but increases in profiles with adverse pressure gradients, $P < 0$. For a detailed description of the

effect of non-parallelism in the analysis, see Saric & Nayfeh [29]. As first shown by Squires [30], the critical Reynolds number is associated with a two-dimensional wave. This fact has lead to the incorrect popular belief that two dimensional disturbances are most unstable at all values of wavenumber α, or frequency F. In our analysis, we restrict our attention to two-dimensional TS waves since this type is most easily produced by the vibrating ribbon technique. The usage of oblique TS waves in our analysis should require little modification. Thus, we drop the z dependence and recast the equations in terms of the disturbance stream function ψ_1. The solution form is given by

$$\psi_1 = A(X)\,[\phi(y)e^{i\alpha_r(X-ct)} + \phi^{\dagger}(y)e^{-i\alpha_r(X-ct)}] \tag{8}$$

The † denotes the complex conjugate, c is the phase velocity, $\alpha = \alpha_r + i\alpha_i$ and $\phi(y)$ are solutions to the Orr-Sommerfeld eigenvalue problem,

$$\begin{gathered}(D^2 - i\alpha R((U_0 - c)D - U_0''))\phi = 0 \\ \phi(0) = \phi'(0) = 0 \quad , \quad \phi(\to\infty) = \phi'(\to\infty) = 0\end{gathered} \tag{9}$$

where $D = \dfrac{d^2}{dy^2} - \alpha^2$ and α_r is the streamwise wavenumber, α_i is the growth rate. Note that R is a coefficient in (9), so that $\alpha = \alpha(R)$ and, consequently, α is also a function of the streamwise position X. The variation of the amplitude is given by

$$A(X) = A_{in}\exp\left(-\int_{X_{in}}^{X} \alpha_i(X)\,dX\right) \tag{10}$$

where A_{in} is the TS amplitude at an initial location X_{in}. In the presence of a TS wave of finite amplitude, the two-dimensional flow has the form

$$\mathbf{v}_2(X,y,t) = \mathbf{V}_o(y) + A(X)\,\mathbf{v}_1(X - ct, y) \tag{11}$$

The eigenfunction $\phi(y)$ in (8) is normalized such that A measures the streamwise rms fluctuation of the disturbance. As the primary disturbance grows from infinitesimal to finite amplitude, nonlinear interactions begin to modify both the mean and the disturbance profiles. However, the numerical studies of Orszag [26] and Herbert [4] in plane Poiseuille flow have shown that nonlinear modifications have negligible effect on the growth of secondary instabilities. Thus, we keep the shape of the TS wave as given by the linear analysis up through finite amplitude values. This approximation is called the shape assumption.

In view of the weak (viscous) growth of the TS wave in comparison to the explosive (convective) growth of secondary disturbances, we neglect the weak variation of the TS amplitude and consider, locally, $A(X) = A(X_o) = A_o$. One may view this approximation as an extension of the parallel flow assumption to the TS wave, and as the 0^{th} order approximation in a weakly non-parallel analysis. The time dependence is eliminated by changing from a fixed coordinate system to a coordinate system moving with the phase velocity of the TS wave, $x = X - ct$, and the flow becomes periodic in the moving streamwise coordinate x,

$$\tilde{\mathbf{v}}_2(x,y) = \mathbf{V}_o(y) + A_o\tilde{\mathbf{v}}_1(x,y) \tag{12}$$

Here, and elsewhere, the $\tilde{}$ symbolizes the periodicity of the function.

Fig. 3 illustrates the above steps. In a neighborhood of X_o both the Falkner-Skan profile and the TS wave amplitude are assumed constant, thereby extending the periodic flow from $-\infty$ to ∞. A detailed study of

temporally and spatially growing TS waves for Falkner-Skan profiles has been presented by Wazzan et al. [31]. The periodic basic flow (12) can be considered as known from any standard procedure for analysis of TS waves.

2. Secondary Disturbances. Linear model.

We study the evolution of secondary disturbances through a linear stability analysis of the periodic basic flow (12). A small secondary disturbance $\mathbf{v}_3 = (u_3, v_3, w_3)$ is superimposed on the basic flow,

$$\mathbf{v}(x,y,z,t) = \tilde{\mathbf{v}}_2(x,y) + \epsilon \mathbf{v}_3(x,y,z,t) \quad , \qquad \epsilon \ll 1 \tag{13}$$

and the compound flow is inserted into the Navier-Stokes equations. The nonlinear convective term $\epsilon^2 (\mathbf{v}_3 \cdot \nabla)\mathbf{v}_3$ is dropped in view of the small disturbance amplitude, yielding linear equations for $\mathbf{v}_3$,

$$\frac{\partial}{\partial t}\mathbf{v}_3 + (\tilde{\mathbf{v}}_2 \cdot \nabla)\mathbf{v}_3 + (\mathbf{v}_3 \cdot \nabla)\tilde{\mathbf{v}}_2 = -\nabla p_3 + \frac{1}{R}\nabla^2 \mathbf{v}_3 \tag{14a}$$

$$\nabla \cdot \mathbf{v}_3 = 0 \tag{14b}$$

subject to the boundary conditions $\mathbf{v}_3(x,0,z,t) = 0$, $\mathbf{v}_3(x,\ y \to \infty\ ,z,t) = 0$. The linear secondary stability problem, hence, is an eigenvalue problem. Taking the curl of (14a) to eliminate the pressure, introducing $\varsigma_1 = -\nabla^2 \psi_1$ and the disturbance vorticity $\omega_3 = (\xi_3, \eta_3, \varsigma_3)$, and using continuity to eliminate the z-component of velocity w_3, we obtain a system of of linear differential equations for u_3 and v_3,

$$\left[\frac{1}{R}\nabla^2 - (U_o - c)\frac{\partial}{\partial x} - \frac{\partial}{\partial t}\right]\nabla^2 v_3 + \frac{d^2 U_o}{dy^2}\frac{\partial v_3}{\partial x} +$$

$$A\left[\left(\frac{\partial \psi_1}{\partial x}\frac{\partial}{\partial y} - \frac{\partial \psi_1}{\partial y}\frac{\partial}{\partial x}\right)\nabla^2 v_3 + \frac{\partial^2 \psi_1}{\partial x^2}\left(\frac{\partial \varsigma_3}{\partial y} + \frac{\partial \eta_3}{\partial z}\right) - \frac{\partial^2 \psi_1}{\partial x \partial y}\left(\frac{\partial \varsigma_3}{\partial x} + \frac{\partial \xi_3}{\partial z}\right) - \right.$$

$$\left. \frac{\partial \varsigma_1}{\partial x}\left(2\frac{\partial u_3}{\partial x} + \frac{\partial v_3}{\partial y}\right) - \frac{\partial \varsigma_1}{\partial y}\frac{\partial v_3}{\partial x} - \left(u_3\frac{\partial}{\partial x} + v_3\frac{\partial}{\partial y}\right)\frac{\partial \varsigma_1}{\partial x}\right] = 0 \tag{15a}$$

$$\left[\frac{1}{R}\nabla^2 - (U_o - c)\frac{\partial}{\partial x} - \frac{\partial}{\partial t}\right]\frac{\partial \eta_3}{\partial z} - \frac{dU_o}{dy}\frac{\partial^2 v_3}{\partial z^2} + A\left[- \frac{\partial^2 \psi_1}{\partial y^2}\frac{\partial^2 v_3}{\partial z^2} + \right.$$

$$\left.\left(\frac{\partial \psi_1}{\partial x}\frac{\partial}{\partial y} - \frac{\partial \psi_1}{\partial y}\frac{\partial}{\partial x} - \frac{\partial^2 \psi_1}{\partial x \partial y}\right)\frac{\partial \eta_3}{\partial z} + \frac{\partial^2 \psi_1}{\partial x^2}\left(\frac{\partial^2 u_3}{\partial x \partial y} + \frac{\partial^2 v_3}{\partial y^2}\right)\right] = 0 \qquad (15b)$$

Note that $\partial \eta_3/\partial z$ and $\partial \xi_3/\partial z$ are expressible in terms of u_3 and v_3 . These equations have three important features: linearity, coefficients independent of time and spanwise coordinate z, and coefficients periodic in x due to the presence of $\tilde{\mathbf{v}}_1$. The first two allow the use of normal modes in t and z,

$$\mathbf{v}_3(x,y,z,t) = e^{i\beta z} e^{\sigma t}\, \hat{\mathbf{v}}_3(x,y) \qquad (16)$$

where the spanwise wavenumber β is real, and σ is in general complex. Floquet theory is fully developed in the context of ordinary differential equations, and is well documented in the literature (see for example Nayfeh & Mook [32], or Arscott [33]). The extension to partial differential equations requires sophisticated mathematics, but seems to provide very similar basic results. In our problem we assume a solution of Floquet form, since, apart from the y dependence, the secondary disturbance equations are essentially of Hill type in x. Letting γ denote the characteristic exponent, and $\lambda_x = 2\pi/\alpha_r$ the TS wavelength, we find two classes of solutions $\hat{\mathbf{v}}_3$ in the form

$$\hat{\mathbf{v}}_3(x,y) = e^{\gamma x}\, \tilde{\mathbf{v}}_f(x,y) \qquad \tilde{\mathbf{v}}_f(x+\lambda_x,y) = \tilde{\mathbf{v}}_f(x,y) \qquad (17a)$$

$$\hat{\mathbf{v}}_3(x,y) = e^{\gamma x}\, \tilde{\mathbf{v}}_s(x,y) \qquad \tilde{\mathbf{v}}_s(x+2\lambda_x,y) = \tilde{\mathbf{v}}_s(x,y) \qquad (17b)$$

where we denote $\tilde{\mathbf{v}}_f(x,y)$ as the "fundamental" mode, and $\tilde{\mathbf{v}}_s(x,y)$ as the "subharmonic" mode. Being periodic, $\tilde{\mathbf{v}}_f$ and $\tilde{\mathbf{v}}_s$ can be represented by Fourier series,

$$\tilde{\mathbf{v}}_f(x,y) = \sum_{n=-\infty}^{\infty} \bar{\mathbf{v}}_{2n}(y) e^{i2n\hat{\alpha}x} \qquad \hat{\alpha} = \alpha/2 \tag{18a}$$

$$\tilde{\mathbf{v}}_s(x,y) = \sum_{n=-\infty}^{\infty} \bar{\mathbf{v}}_{2n+1}(y) e^{i(2n+1)\hat{\alpha}x} \tag{18b}$$

In principle, we can arrive at the same result by first expressing the solution in a Fourier series in $\hat{\alpha}$,

$$\mathbf{v}_3(x,y,z,t) = e^{i\beta z} e^{\sigma t} e^{\gamma x} \sum_{n=-\infty}^{\infty} \bar{\mathbf{v}}_n(y) e^{in\hat{\alpha}x} \tag{19}$$

and then introducing the basic flow (12) and secondary disturbance (19) into the equations (15). The terms multiplied by exponentials of like index are collected and set equal to zero, two uncoupled infinite sets of equations result for the fundamental components $\bar{\mathbf{v}}_{2n}(y)$ and subharmonic components $\bar{\mathbf{v}}_{2n+1}(y)$. Due to the extensiveness of algebra involved, these equations have been relegated to the appendix.

The solution forms (17a,b) reproduce the experimentally observed behavior of three-dimensional disturbances [1,3]. The fundamental mode produces the λ_z-periodic "in-line" or peak-valley splitting pattern as observed by Saric & Thomas [9, Fig. 1]. The aperiodic term $\bar{\mathbf{v}}_0(y)$ in the series (17a) gives rise to both a mean flow distortion and a spanwise periodic longitudinal vortex structure. The subharmonic mode produces the $2\lambda_z$-periodic staggered structure [9, Fig. 2, 3] and has no aperiodic term in the series (17b). Both the fundamental and subharmonic modes can undergo exponential growth in time or space, consistent with experience from numerical simulations and experiments (see also [34]).

The secondary instability equations can be recasted with real coefficients, since the Navier-Stokes equation involves only real values.

Thus, the eigenvalues are either real, or complex conjugates. In the case of complex eigenvalues special care must be taken in the computational technique to follow the birth and collapse of the complex parts. For real eigenvalues, the method of solution herein presented is valid, and the use of a real formulation provides considerable savings in the numerical work.

3. Spatial and temporal growth in a moving frame

Owing to the exponential dependence of $\mathbf{v}_1$ on both time and space, as seen in (19), we are faced with the necessity of choosing one of the exponents , σ or γ, as the eigenvalue. In this manner we select between temporally growing or spatially growing modes, in full similarity to the study of TS waves. Temporal growth analysis is simpler and requires less computational effort since σ appears linearly in the equations, while γ appears up to fourth power. Moreover, a relation exists between the two types of growth, and can be utilized to approximately transform temporal into spatial growth rates (see below).

For primary disturbances, spatial growth is measured with respect to the laboratory frame of coordinates. In order to arrive at a consistent formulation of temporal and spatial amplification for secondary modes, we express the velocity field (19) in laboratory coordinates

$$\mathbf{v}_3(X,y,z,t) = e^{i\beta z} e^{(\sigma - \gamma c)t} e^{\gamma X} \sum_{n=-\infty}^{\infty} \bar{\mathbf{v}}_n(y)\, e^{in\hat{\alpha}(X - ct)} \qquad (20)$$

To restrict the disturbance exclusively to temporal amplification we set the "spatial" exponent γ to zero and solve for the "temporal" exponent σ as an eigenvalue. The real part of σ dictates growth and decay in both

coordinate systems, hence the moving and the laboratory-fixed observer witness the same temporal growth. For purely real σ, the mode is fixed in the (x,y,z,t) frame and, hence, tuned with the TS wave. For complex σ one obtains conjugate pairs, $\sigma = \sigma_r \pm \sigma_i$, and the modes propagates upstream and downstream in the moving coordinate system. In a laboratory fixed frame the disturbances travel with a phase speed different from that of the TS wave. Calculations have shown that at realistic amplitudes the dominant, i. e. most unstable, mode is associated with a real eigenvalue.

A spatially amplified disturbance in the *moving* coordinate system can be computed by setting σ equal to zero and solving for γ as an eigenvalue. To a *laboratory-fixed* observer, however, this disturbance mode exhibits mixed spatial-temporal amplification, since in (15) both σ and γ are multiplied by time.

The two cases of most interest are those of either temporal or spatial amplification in laboratory coordinates. Indeed, experimental observation shows that in boundary layers the growth of primary and secondary disturbances is only spatial.

In order to obtain disturbance modes with purely spatial amplification in the laboratory frame, we note from (20) that the time-dependent factor $e^{(\sigma-\gamma c)t}$ can be suppressed by choosing $\sigma = \gamma c$. In the moving frame, we therefore search for solutions of the form

$$\mathbf{v}_3(x,y,z,t) = e^{i\beta z} e^{\gamma c t} e^{\gamma x} \sum_{n=-\infty}^{\infty} \bar{\mathbf{v}}_n(y) e^{in\hat{\alpha}x} \tag{21}$$

and solve for γ as the eigenvalue. (Recall that computations must be carried out in the moving coordinate system for only there is the Floquet theory

directly applicable). We calculated all the information on spatially growing modes in this report using this approach. Lastly, we note that setting $\sigma = \gamma c + \Delta$ produces disturbances growing spatially in X but having the frequency detuned from the subharmonic by the value of Δ. In this case the eigenvalue γ is complex, with the imaginary part producing the modification of the streamwise wavenumber associated with the change in frequency.

NUMERICAL METHODS

The Falkner-Skan equation (2), the OSE (9) , and the secondary disturbance equations (14) are numerically solved.

The Falkner-Skan profile $f(y)$ is calculated using a 4^{th} order Runge-Kutta integrator coupled with a shooting scheme to satisfy the boundary condition at infinity. An accurate value of $f''(0)$, necessary to initiate the shooting procedure, is obtained from a parabolic fit of $f''(0)$ as function of P from existing data [35], thus minimizing the number of iterations, and, more importantly, avoiding the calculations of profiles with backflow [35] in adverse pressure conditions, $-0.198 < P < 0$.

For the fundamental and subharmonic profiles (18) the lowest Fourier truncation is used: $\mathbf{v}_{-2},\mathbf{v}_0,\mathbf{v}_2$ for the fundamental, and $\mathbf{v}_{-1},\mathbf{v}_1$ for the subharmonic. The dominance of the first terms in the series and the small error of the truncation have been proven in previous works [36], [37]. Both the OSE and the secondary disturbance equations are solved by transforming the differential equations into an algebraic form through the use of a spectral collocation method with Chebyshev polynomials [38]. In view of the finite domain of definition for Chebyshev polynomials, the semi-infinite domain $y \in [0,\infty)$ is mapped into $\hat{y} \in [1,0)$ by the transformation $y = \frac{y_o}{\hat{y}} - y_o$. Letting K denote the number of collocation points used in the analysis, one chooses the value of y_o such that half the collocation

points $\hat{y}_k = \cos(\frac{k\pi}{2K+2})$ are placed inside the boundary layer displacement thickness, wherein the disturbances undergo rapid change.

Without loss of generality, we use the subharmonic instability problem to discuss in detail some aspects of the numerical method. We approximate the eigenfunctions $\vec{v}_n = (u_n , v_n)$ in series expansion (18) by a finite series of odd Chebyshev polynomials,

$$u_n(\hat{y}) = \sum_{k=1}^{K+1} a_{nk} T_{2k+1}(\hat{y}) \quad , \quad v_n(\hat{y}) = \sum_{l=1}^{K+2} b_{nl} T_{2l+1}(\hat{y}) \qquad (22)$$

The use of only odd polynomials, all of which vanish at $\hat{y} = 0$, causes the boundary conditions at that end, which is the image of $y = \infty$, to be automatically satisfied. Substituting the Chebyshev series representation of the velocity components into the governing equations and solving the equations at the K collocation points results in a $4K$ row by $4K + 6$ column algebraic system for the unknown coefficients a_{nk} and b_{nl}. The system is made solvable (square matrix) by the addition of the algebraic form of the six boundary conditions at $\hat{y} = 1$, which is the image of the wall at $y = 0$,

$$u_n = 0 \ , \ v_n = 0 \ , \ \frac{dv_n}{d\hat{y}} = 0 \qquad (23)$$

For elegance, and computational simplicity, the "chain rule terms" arising from the algebraic mapping are incorporated in the definition of the derivatives of the Chebyshev polynomials. The ability to do this is based. clearly. on the linearity of the equations; for example,

$$\frac{dv_n}{dy} = -\frac{\hat{y}^2}{y_o}\frac{dv_n}{d\hat{y}} = \sum b_{nl}\left[\frac{-\hat{y}^2}{y_o}\right]\frac{d}{d\hat{y}} T_{2l+1}(\hat{y})$$

$$= \sum b_{nl}\frac{d}{d\hat{y}}\hat{T}_{2l+1}(\hat{y}) \qquad (24)$$

The advantage of solving the problem in its original boundary value format, versus solving it via a shooting technique, is great. A global eigenvalue search procedure, such as EISPACK (Smith et al [39]) can be applied to the algebraic system to obtain a complete spectrum of the eigenvalues at new locations in the multidimensional parameter space (α,β,R,A). Choosing from the global list a most interesting eigenvalue, one can then compute its variation during a local walk in the multidimensional space. A Newton iteration procedure is used, which computationally less demanding: order $(4K+6)^3$ versus order $(4K+6)^4$ for EISPACK.

A discussion of the local procedure can be easily done by introducing the following notation. We represent the algebraic formulation of the problem by

$$G[\mathbf{y}] = 0 \tag{25}$$

where $\mathbf{y}$ is the p-dimensional vector composed of the unknown coefficients,

$$\mathbf{y} = (a_{1k}\ ,\ b_{1l}\ ,\ a_{-1k}\ ,\ b_{-1l}) \tag{26}$$

$$k = 1\ ,\ K+1 \quad ,\quad l = 1\ ,\ K+2 \quad ,\quad p = 2(K+1) + 2(K+2)$$

and $G : \mathbf{R}^p \rightarrow \mathbf{R}^p$ is the linear operator, acting on $\mathbf{y}$, constructed by the spectral collocation method. The eigenvalue σ appears linearly in G, while γ appears up to fourth power. For generality, we let λ denote either of the eigenvalues and indicate the functional dependence of G on λ by writing G_λ.

The local procedure is based on the property that the eigenvalue λ and the eigenvector $\mathbf{y}$ are smooth functions of the parameters $(\alpha\ ,\ \beta\ ,\ R\ ,\ A)$. Thus, given an exact pair $\lambda_o\ ,\ \mathbf{y}_o$ at $(\alpha_o\ ,\ \beta_o\ ,\ R_o\ ,\ A_o)$ we search for

λ_* , $\mathbf{y}_*$ at $(\alpha_o + \Delta\alpha\ ,\ \beta_o + \Delta\beta\ ,\ R_o + \Delta R\ ,\ A_o + \Delta A)$ via Newton iteration. To this end, we augment the system by constructing

$$\mathbf{x} = (\mathbf{y}\ ,\ \lambda) \qquad\qquad \mathbf{x} \in \mathbf{R}^{p+1} \tag{27}$$

and $F_\lambda : \mathbf{R}^{p+1} \rightarrow \mathbf{R}^{p+1}$ is obtained by adding to G an eigenvector normalization condition (for example, setting the last coefficient, b_{-1L}, equal to 1). Note that F is not a linear operator when λ represents γ, i.e in a spatial formulation. Via a Taylor series expansion we write,

$$0 = F(\mathbf{x}_o) \ + \ \nabla F_{\mathbf{x}_o}[\mathbf{x}_* - \mathbf{x}_o] \ + \ O(\ |\mathbf{x}_* - \mathbf{x}_o\ |^2) \tag{28}$$

where $\nabla F_{\mathbf{x}_o}$ is the Jacobian evaluated at $\mathbf{x}_o$, acting on $\mathbf{x}_* - \mathbf{x}_o$. Omitting the higher order terms we rewrite the equation in the form

$$\nabla F_{\mathbf{x}_{\nu-1}}[\mathbf{x}_\nu - \mathbf{x}_{\nu-1}] = F(\mathbf{x}_{\nu-1}) \tag{29}$$

and solve for $\mathbf{x}_\nu$ iteratively. As written, the Jacobian is updated at each iteration, yielding a convergence rate of second order at a computational cost of order p^3. Suppressing the updating to selected intervals gives a convergence rate of first order, but decreases the computational labor to order p^2. Since 20 to 30 collocation points are necessary for good accuracy, the value of p is between 86 and 126, so that the selected updating of the Jacobian can greatly reduce the numerical work.

RESULTS

1. Introduction

In low turbulence conditions, such as those that exist in free flight, the subharmonic type of secondary disturbance is much more unstable than the fundamental type (Klebanoff structure) [40]. This fact, together with the need of extensive computer time for a detailed study, led us to focus our attention exclusively on the subharmonic modes. The study of pressure gradient on subharmonic disturbances is complicated by the functional dependence of the eigenvalues λ (*growth rates*) on a large number of parameters,

$$\lambda = \lambda\,(\alpha\,,\,\beta\,,\,R\,,\,A\,,\,P) \tag{30}$$

A significant portion of the research was employed for orientation in this multi-dimensional space. Hence, as a preparation for discussion of the results, it is useful to mention the most interesting choices of parameter variation. The spanwise wavenumber selectivity, given by the variation of growth rate with β, addresses the question of two or three-dimensionality of the disturbance. This variation is included in almost all the graphs. To take into account the change of the nondimensionalizing variable δ with streamwise location we replace β with the variable b

$$b = 1000\,\beta\,/\,R$$

which describes a wave of fixed physical spanwise wavenumber as it travels downstream. Other important parameters are the TS amplitude, the pressure coefficient P, and the Reynolds number. The influence of at most two parameters can be clearly represented in a graph. The following combinations are presented:

- α , R , A *fixed* ; b , P *varied.*
- α , R , P *fixed* ; b , A *varied.*
- α , P , A *fixed* ; b , R *varied.*
- β , R , A *fixed* ; b , α *varied.*

The value of α is a specified parameter in temporal analysis, and the TS wave frequency ω, is given as the imaginary part of the eigenvalue of the OSE. As done above, we define a new frequency , F, independent of the downstream change of the nondimensionalizing variable δ,

$$F = 10^6 \, \omega \, / \, R$$

In spatial analysis, the value of the frequency F is specified, and the TS wave wavenumber α_r is given as the real part of the eigenvalue of the OSE. Hence note that the functional dependence on α in (30) is changed to F when dealing with results from the spatial analysis. The spatial calculations were conducted mainly at $F = 124$ and $F = 83$ to match experimental conditions [8],[41].

2. Effect of pressure gradient

We begin the discussion of results by presenting a comparison between theory and experiment to validate the accuracy of the theoretical model. Fig. 4 juxtaposes experimental [8] and theoretical results for the spatial

amplitude growth of TS wave and subharmonic mode for the Blasius profile. The initial TS amplitude is $A_{in} = 0.44\%$ at branch I, ($R_I = 535$) and grows to 1.23% at branch II ($R_{II} = 855$). A virtual leading-edge correction of 20 cm has been applied to the experimental data in order to bring the experimental $R_{II} = 840$ into agreement with the theoretical value, 855.

The initial subharmonic amplitude was chosen at $B_{in} = 0.00126\%$ in order to match the experimental value of B at R_{II}. The subharmonic amplitude is calculated using

$$\ln\left(\frac{B}{B_o}\right) = \int_{R_o}^{R} \gamma(s) \frac{2}{2 - P} ds$$

For data points at $R > 700$ the computed growth rate closely follows the observed slope, confirming the parametric nature of subharmonic instability in the initial stages of growth. The measurements at $R < 700$ were taken shortly downstream of the vibrating ribbon (R =575) where neither the TS wave nor the subharmonic mode are fully established. Fig. 5 shows the selectivity of the subharmonic instability mechanism with respect to b at R =700 and 853. Based on the maximum spatial growth rate, the theory predicts $b = 0.27$ at $R = 700$ and $b = 0.29$ at $R = 855$. However, natural selection of b in experiments also depends on the spectral content of the background noise. The observed value of $b = 0.33$ is close to maximum amplification throughout the range of measurement.

Fig. 4 and 5 are almost indistinguishable from those given in a previous comparison [2, Fig. 9, 13] in which the growth rates are computed using a temporal formulation and converted to the experimentally observed spatial

growth rates by means of a simple transformation. We devote an entire section to the the comparison of spatial and temporal data.

A detailed collection of experimental data for transition over surfaces with an adverse pressure gradient is, today, unavailable. This is unfortunate because the anticipated increase in the error due to the shape and quasi-static assumptions cannot be assessed by comparison. Indeed there is evidence [42] that near separation the distortion of the mean flow is not negligible. However, we expect the current results to capture accurately the quantitative behavior of the growth rates.

The destabilizing effect of an adverse pressure gradient on the dominant subharmonic mode is shown in Fig. 6. A decrease in the pressure coefficient increases the growth rate as well as the range of unstable spanwise wavenumbers. A likely consequence of this effect is the amplification of a relatively narrow band of spanwise wavenumbers in regions of favorable pressure gradients, which sets the stage for the downstream development. Most surprising in Fig. 6 is the sharp cutoff at $b \approx 0.05$ for the inflectional profiles, indicating strong damping of the vortex pairing mode at a TS amplitude of 1%. Detuned modes (σ complex) are less amplified than the dominant mode in all profiles and at all values of the TS amplitude we have investigated.

While the adverse pressure gradient enhances the growth rates of both the TS wave and the subharmonic disturbance, there is only a moderate effect on qualitative features. Dramatic changes occur, however, in the eigenfunctions, i. e. in the disturbance velocity profiles. A comparison of mean and streamwise rms profiles is given in Fig. 7 for the Blasius profile.

$P = 0$, and in Fig. 8 for the Falkner-Skan profile near separation, $P = -0.18$. Fig. 7 shows the agreement of the spatial result for the subharmonic mode with the experimental data [8]. Comparison with [2, Fig. 14] also indicates that spatial and temporal results for the velocity profiles are hardly distinguishable. The position of the maxima with respect to the critical layer at y_c (for the TS wave below, and for the subharmonic mode above y_c) is qualitatively unaffected by the pressure gradient. However, y_c in Fig. 8 is further away from the wall. A second maximum develops in the TS profile owing to the gradual changeover from viscous to vortical (inviscid inflectional) instability. Velocity profiles at values of $R = 1168$ and $F = 83$ are shown in Fig. 9. We note by comparison to the profiles at $R = 873$ that only a small modification is brought about by a change in frequency and Reynolds number. Experimental data on disturbance velocities are scarce. At the present, we can only say that our results are not inconsistent with measurements [42, Fig. 14] in the separating flow over an airfoil.

3. Comparison of wall-bound and free shear layers

Boundary layer profiles near the point of separation exhibit high inflectionality and maximum shear stress far from the wall, thus bearing resemblance to a free shear layer. This observation leads one to enquire under which conditions the two types of flow share stability characteristics. In the light of separation and reattachment we place particular attention on the preferred spanwise wavelength of subharmonic modes, in other words, on the two-dimensional or three-dimensional nature of secondary distur-

bances.

The inviscid stability of a spatially periodic free-shear layer has been studied numerically by Pierrehumbert & Widnall [20]. They found the layer to be most unstable with respect to a two-dimensional ($\beta = 0$) subharmonic mode, and the growth rate monotonically decreasing with increasing β [20, Fig. 5]. The disturbances undergo pure exponential growth and are tuned (σ real).

Growth rates for the pairing mode and a three-dimensional subharmonic mode in the Falkner-Skan profile at separation are shown in Fig. 10 as a function of the TS amplitude. Under these conditions, three-dimensional secondary instability is dominant up to TS amplitudes of 18%. At low amplitudes, the vorticity concentrations generated by the TS wave are too feeble to overcome the damping effect of the wall on the pairing mode. Vortex pairing takes the lead at very large amplitudes of the primary disturbance, but still competes with three-dimensional phenomena. This is more clearly shown by the growth rates as a function of the spanwise wavenumber b in Fig. 11. There is a strong similarity between the curve for $A = 30\%$ and the curve in [20, Fig. 5] for amplitudes in the same range. Note, however, that the neglection of nonlinear terms under the shape assumption may be invalid at this high amplitude level. The effect of the increase of vorticity on the streamlines can be seen on Fig. 12. At amplitude of 1% the vorticity concentration at the critical layer is weak, creating a streamline pattern greatly flattened by the presence of the wall. At amplitude of 30%, however, the effect of the wall is not pronounced and the streamlines resemble closely those of a free vortex. This process is accom-

panied by the stability changeover to a basically inviscid vortical mechanism.

As a further check that detuned modes are always less amplified than tuned modes a comparison of growth rates was made for different values of α. For the separation profile ($P = -0.198$), Fig. 13 shows the growth rate of the *most unstable* fixed mode together with the two dimensional ($\beta = 0$) running mode as a function of α. For the most unstable fixed mode β varies from 0.34 at $\alpha = 0.5$, to 0.08 at $\alpha = 0.05$. Clearly, as α is decreased from the upper branch to the lower branch of the TS neutral curve this mode always dominates in growth rate.

Since the large TS amplitudes required for the pairing mode to dominate can hardly be reached by viscous growth, we can conclude that within the entire attached boundary layer the development of secondary instabilities, and hence the second stage of transition, will be dominated by three-dimensional disturbances. Through this result it is fair to observe that the process of vortex pairing in the separated shear layer is controlled not by the growth of vortex pairing prior to separation but by the amplitude growth of the three-dimensional disturbances. This observation is substantiated by experiments in free shear layers [43] in which vortex pairing was observed to dominate only when the background disturbances where sufficiently low (hence, low amplitudes of the three-dimensional disturbances in the boundary layer over the splitter plate).

4. Temporal to spatial transformation for secondary disturbances

In view of the reduced computational effort needed for a temporal eigenvalue search, as opposed to a spatial search, a natural interest arises in

a transformation relating the two types of growth rates.

Indeed, one may even hope for the existence of a simple and accurate relation valid over a wide subdomain of the parameter space since, after all, such is the case for primary (TS) disturbances (Gaster's transformation [44]. For a transformation in non-parallel flows, see [45]).

The transformation for secondary disturbances can be derived in a straight forward manner, as shown below. Unfortunately, the transformation takes on a simple form only in regions near a neutral growth point, where both growth rates are small. The transformation acquires an involved form in regions of large growth rates, and the substantial amount of computation required may undercut its usefulness.

In the moving coordinate system (ξ,y,z,t) the velocity field solution to the secondary disturbance equations takes the form

$$\mathbf{v}_3(\xi,y,z,t) = e^{i\beta z}e^{\sigma t}e^{\gamma\xi}\sum_{n=-\infty}^{\infty}\bar{\mathbf{v}}_n(y)e^{in\hat{\alpha}\xi} \tag{30}$$

where σ and γ are the complex temporal and spatial growth rates, respectively, and α and β are the streamwise and spanwise wave numbers, respectively. We recall that solutions with

$$\left.\begin{array}{l}\sigma = \sigma_r + \sigma_i \\ \gamma = 0\end{array}\right\} \quad \textit{represent temporal growth in both fixed and moving coordinate systems} \tag{31a}$$

$$\left.\begin{array}{l}\sigma = \gamma c \\ \gamma = \gamma_r + \gamma_i\end{array}\right\} \quad \textit{represent spatial growth in fixed coordinates} \tag{31b}$$

The disturbance equations functionally relate the parameters γ,σ,α, and β in the implicit form

$$F(\gamma,\sigma,\alpha,\beta) = 0 \tag{32}$$

provided that all other parameters appearing in the equations, namely R, frequency, T-S amplitude, and pressure coefficient P, remain constant.

We will henceforth assume that the polysurface described by equation F is smooth and the partial derivatives with respect to its variables exist up to the order required.

Seeking a transformation from temporal to spatial growth we re-write (32) in the explicit form

$$\gamma = f(\mathbf{r}), \qquad \mathbf{r} = (\sigma,\alpha,\beta)$$

We choose two points $\mathbf{r}_s$ and $\mathbf{r}_t \in (\sigma,\alpha,\beta)$, and connect them with a smooth path $\mathbf{c}(p)$ parametrized by p, with end points $\mathbf{c}(0) = \mathbf{r}_t$ and $\mathbf{c}(1) = \mathbf{r}_s$. The values of γ at the two end points of the path are related by the first fundamental theorem of calculus,

$$\gamma(\mathbf{r}_s) - \gamma(\mathbf{r}_t) = \int_0^1 grad(F) \cdot \frac{d\mathbf{c}(t)}{dp} dt \tag{33}$$

This is a most general transformation. In the special case when $\mathbf{r}_s$ and $\mathbf{r}_t$ correspond to spatial and temporal growth rates respectively, the end points are according to (31),

$$\mathbf{r}_s = (\gamma^o c,\alpha,\beta) \quad \text{and} \quad \mathbf{r}_t = (\sigma^o,\alpha,\beta)$$

where γ^o is the spatial and σ^o the temporal growth rate. The path $\mathbf{c}(p)$ now keeps the value of α and β constant, and (33) reduces to

$$\gamma^o = \int_{\sigma^o}^{\gamma^o c} \left[\frac{\partial}{\partial\sigma_r}\gamma_r + i\frac{\partial}{\partial\sigma_r}\gamma_i\right] d\sigma_r \tag{34}$$

where use has been made of the Cauchy - Riemann condition

$$\frac{\partial \gamma}{\partial \sigma} = \frac{\partial \gamma_r}{\partial \sigma_r} + i \frac{\partial \gamma_i}{\partial \sigma_r} = \frac{\partial \gamma_i}{\partial \sigma_i} - i \frac{\partial \gamma_r}{\partial \sigma_i} \tag{35}$$

Equation (34) is the desired transformation. Note that the spatial eigenvalue, which is the unknown, appears on both sides of the transformation. Next we want to reduce equation (34) to a form involving only data obtained at, or near, the endpoint c (0) corresponding to temporal growth. Therefore, we expand the integrand in a Taylor series about σ_r^o

$$\frac{\partial}{\partial \sigma_r}\gamma_r(\sigma_r) = g_o + g_o'(\sigma_r - \sigma_r^o) + \frac{g_o''}{2}(\sigma_r - \sigma_r^o)^2 + \ldots \tag{36}$$

where

$$g_o = \frac{\partial}{\partial \sigma_r}\gamma_r(\sigma_r^o) \quad , \quad g_o' = \frac{\partial^2}{\partial \sigma_r^2}\gamma_r(\sigma_r^o) \quad , \quad \textit{etc.} \tag{37}$$

Inserting the Taylor series into (5) we obtain the following approximate transformations for real eigenvalues,

One term :

$$\gamma_r^o = \int_{\sigma_r^o}^{\gamma_r^o c} g_o \, d\sigma_r$$

$$\gamma_r^o = \frac{\sigma_r}{(c - \frac{1}{g_o})} \tag{38a}$$

Two term :

$$\gamma_r^o = \int_{\sigma_r^o}^{\gamma_r^o c} \left\{ g_o + g'_o(\sigma_r - \sigma^{o_r}) \right\} d\sigma_r$$

$$a_2 \gamma_r^2 + a_1 \gamma_r + a_o = 0 \tag{38b}$$

where

$$a_2 = g'_o c^2$$

$$a_1 = (g_o - g'_o \sigma_r^o)c - 1$$

$$a_o = g'_o(\sigma_o^o)^2 - g_o\sigma_r^o$$

A three-term Taylor series yields a cubic algebraic equation for γ_r^o, a four-term series yields a quartic, and so on. Since approximations of higher order require numerous values of $\gamma = \gamma(\sigma)$ near, and at, σ_r^o for the calculation of higher derivatives and also require numerical solution to the associated algebraic equation, high order approximations become too cumbersome to calculate. The results for a one-term and two-term transformation are given below. Blasius flow $\mathrm{Re} = 1168$, $F = 83$, $\alpha = 0.276$, $A \tilde{=} 1\%$

Exact Values		
β	σ^{o_r} $\times 10^2$	γ^{o_r} $\times 10^2$
0.042	0.000	0.000
0.09	0.775	2.117
0.18	1.175	3.188
0.32	1.169	3.170

γ from approximate transformations						
β	$\frac{\sigma_r}{c}$	Error %	One term $\times 10^2$	Error %	Two term $\times 10^2$	Error %
0.042	0.000	0	0.000	0	0.000	0
0.09	2.207	4.25	2.094	1.1	2.114	0.1
0.18	3.345	4.93	3.063	4.0	3.137	1.6
0.32	3.328	4.98	3.031	4.5	3.112	1.8

Clearly, for β near the neutral stability point, both the one-term and two-term approximation yield good results. However, away from this point the approximation becomes inaccurate. The error due to truncation is large at higher values of γ_r^o and σ_r^o, where the function $\gamma = \gamma(\sigma)$ exhibits strong curvature. This can be seen in Fig. 14. The function $\gamma = \gamma(\sigma)$ is quasi linear at $\beta = 0.09$ while for higher values of β the curvature undergoes strong bending as it approaches the spatial endpoint $\gamma_r^o c$.

Under strong curvature numerous terms in the Taylor series expansion (34) must be kept for accuracy, and due to the accompanying increase of computational work the transform loses its labor saving advantage. Expansions other than a Taylor series could yield better convergence.

The plot of $\gamma = \gamma(\beta)$ at fixed Re,α,F, and T-S amplitude is shown in Fig. 15, along with the transformed values at three β locations. The zeroth order approximation

$$\gamma_r^o = \frac{\sigma_r^o}{c} \tag{39}$$

is the one used in previous works [2], and gives the error upper bound for values of amplitude less than 2%.

CONCLUSION

The present investigation finds that, under free-flight conditions (low-turbulence) , the secondary disturbances in boundary layers with favorable and adverse pressure gradients (up to separation) behave similarly to those in the Blasius boundary layer, with the most noticeable effect of the pressure gradient being a decrease (favorable) or increase (adverse) of the disturbance's growth rate. In particular, the dominant disturbances are always three-dimensional and tuned (real eigenvalues) to the phase speed of the TS wave. Only at experimentally unreachable amplitudes in the neighborhood of 20-30% does the secondary stability of the boundary layer become similar to that of a free shear layer, whereat the vortex pairing dominates in growth. This fact is of importance, since it is conjectured that the rapid evolution of three-dimensional disturbances prior to the separation of the boundary layer may cause the separated shear layer to break down into wall-bound turbulence.

A comparison of growth rates obtained from a temporal analysis and a spatial analysis shows that the results from the two formulations can be related easily, with an acceptable amount of error, but an involved transformation is necessary for an accurate change. Thus temporal analysis remains a useful tool due to its lower computational demand, and spatial analysis is of use when an accurate comparison with experimental data is needed.

Due to a lack of experimental data for transition in boundary layers with non-constant pressure gradient, a much needed comparison of theory and experiment is not possible. Good agreement in the Blasius boundary layer, however, suggests that at least qualitatively the presented results are valid.

APPENDIX

Herein we substitute the TS streamfunction ψ_1 and the normal mode form of the secondary disturbance (19) into the governing equations (15a,b), and arrive at the final formulation of the problem. First, we divide the differential equations into a sum of operators acting separately on u and v:

Equation (15a),

$$\mathbf{L}(v) = \left[\frac{1}{R}\nabla^2 - (U_o - c)\frac{\partial}{\partial x} - \frac{\partial}{\partial t}\right]\nabla^2 v + \frac{d^2U_o}{dy^2}\frac{\partial v}{\partial x}$$

$$\mathbf{P}^u(\psi,u) = \frac{\partial^2\psi}{\partial x^2}\left(\frac{\partial^2 u}{\partial x^2} - \frac{\partial^2 u}{\partial y^2} + \frac{\partial^2 u}{\partial z^2}\right) + 2\frac{\partial^2\psi}{\partial x\,\partial y}\frac{\partial^2 u}{\partial x\,\partial y} + 2\frac{\partial\nabla^2\psi}{\partial x}\frac{\partial u}{\partial x} + u\frac{\partial^2\nabla^2\psi}{\partial x^2}$$

$$\mathbf{P}^v(\psi,v) = \left(\frac{\partial\psi}{\partial x}\frac{\partial}{\partial y} - \frac{\partial\psi}{\partial y}\frac{\partial}{\partial x}\right)\nabla^2 v + 2\frac{\partial^2\psi}{\partial x^2}\frac{\partial^2 v}{\partial x\,\partial y} + \frac{\partial^2\psi}{\partial x\,\partial y}\left(\frac{\partial^2 v}{\partial y^2} - \frac{\partial^2 v}{\partial x^2} + \frac{\partial^2 v}{\partial z^2}\right) + \frac{\partial\nabla^2\psi}{\partial x}\frac{\partial v}{\partial y} + \frac{\partial\nabla^2\psi}{\partial y}\frac{\partial v}{\partial x} + v\frac{\partial^2\nabla^2\psi}{\partial x\,\partial y}$$

Equation (15b),

$$\mathbf{M}^u(u) = \left[\frac{1}{R}\nabla^2 - (U_o - c)\frac{\partial}{\partial x} - \frac{\partial}{\partial t}\right]\left(\frac{\partial^2 u}{\partial x^2} + \frac{\partial^2 u}{\partial z^2}\right)$$

$$\mathbf{M}^v(v) = \left[\frac{1}{R}\nabla^2 - (U_o - c)\frac{\partial}{\partial x} - \frac{\partial}{\partial t}\right]\frac{\partial^2 v}{\partial x\,\partial y} - \frac{dU_o}{dy}\frac{\partial^2 v}{\partial z^2}$$

$$\mathbf{Q}^u(\psi,u) = \left(\frac{\partial\psi}{\partial x}\frac{\partial}{\partial y} - \frac{\partial\psi}{\partial y}\frac{\partial}{\partial x} - \frac{\partial^2\psi}{\partial x\,\partial y}\right)\left(\frac{\partial^2 u}{\partial x^2} + \frac{\partial^2 u}{\partial z^2}\right) + \frac{\partial^2\psi}{\partial x^2}\frac{\partial^2 u}{\partial x\,\partial y}$$

$$\mathbf{Q}^v(\psi,v) = \left(\frac{\partial\psi}{\partial x}\frac{\partial}{\partial y} - \frac{\partial\psi}{\partial y}\frac{\partial}{\partial x} - \frac{\partial^2\psi}{\partial x\,\partial y}\right)\frac{\partial^2 v}{\partial x\,\partial y} + \frac{\partial^2\psi}{\partial x^2}\frac{\partial^2 v}{\partial y^2} - \frac{\partial^2\psi}{\partial y^2}\frac{\partial^2 v}{\partial z^2}$$

The general form (no truncation) for the TS wave streamfunction is

$$\psi_1 = A \sum_{m=-\infty}^{\infty} \phi_m e^{im\alpha x} \tag{40}$$

The general form (no truncation) for the secondary disturbance equation is

$$\mathbf{v}_3(x,y,z,t) = e^{i\beta z} e^{\sigma t} e^{\gamma z} \sum_{n=-\infty}^{\infty} \bar{\mathbf{v}}_n(y) e^{in\hat{\alpha}x} \tag{41}$$

where $\hat{\alpha} = \alpha/2$ and $\bar{\mathbf{v}}_n = (u_n, v_n)$. Introducing (40) and (41) into equations (15a,b) and collecting terms multiplied by exponentials with like index yields the following infinite sets of equations,

Equation (15a),

$$\mathbf{L}(v_n) + RA \sum_{m=-\infty}^{\infty} [\mathbf{P}^u(\phi_m, u_j) + \mathbf{P}^v(\phi_m, v_j)] = 0 \tag{42a}$$

Equation (15b),

$$\mathbf{M}^u(u_n) + \mathbf{M}^v(v_n) + RA \sum_{m=-\infty}^{\infty} [\mathbf{Q}^u(\phi_m, u_j) + \mathbf{Q}^v(\phi_m, v_j)] = 0 \tag{42b}$$

where $j = n - 2m$

The infinite order system (42a,b) must be truncated for computational reasons. Under the shape assumption, we truncate the TS streamfunction (40) to two terms; ϕ_{-1} and ϕ_1, and for the secondary disturbance the lowest truncation is used; $\mathbf{v}_{-2}, \mathbf{v}_0, \mathbf{v}_2$ for the K-type disturbance (fundamental), and $\mathbf{v}_{-1}, \mathbf{v}_1$ for the subharmonic disturbance. The system (42a,b) separates into two uncoupled equations for the K-type and the subharmonic disturbance:

EQUATIONS FOR K-TYPE

Equation (42a),

$$\begin{aligned} \mathbf{L}(v_2) &+ RA\mathbf{P}^u(\phi_1, u_o) + RA\mathbf{P}^v(\phi_1, v_o) = 0 \\ \mathbf{L}(v_o) &+ RA\mathbf{P}^u(\phi_1, u_{-2}) + RA\mathbf{P}^v(\phi_1, v_{-2}). \\ &+ RA\mathbf{P}^u(\phi_{-1}, u_2) + RA\mathbf{P}^v(\phi_{-1}, v_2) = 0 \\ \mathbf{L}(v_{-2}) &+ RA\mathbf{P}^u(\phi_{-1}, u_o) + RA\mathbf{P}^v(\phi_{-1}, v_o) = 0 \end{aligned}$$

Equation (42b),

$$\begin{aligned} \mathbf{M}^u(u_2) + \mathbf{M}^v(v_2) &+ RA\mathbf{Q}^u(\phi_1, u_o) + RA\mathbf{Q}^v(\phi_1, v_o) = 0 \\ \mathbf{M}^u(u_o) + \mathbf{M}^v(v_o) &+ RA\mathbf{Q}^u(\phi_1, u_{-2}) + RA\mathbf{Q}^v(\phi_1, v_{-2}). \\ &+ RA\mathbf{Q}^u(\phi_{-1}, u_2) + RA\mathbf{Q}^v(\phi_{-1}, v_2) = 0 \\ \mathbf{M}^u(u_{-2}) + \mathbf{M}^v(v_{-2}) &+ RA\mathbf{Q}^u(\phi_{-1}, u_o) + RA\mathbf{Q}^v(\phi_{-1}, v_o) = 0 \end{aligned}$$

EQUATIONS FOR SUBHARMONIC

Equation (42a),

$$\begin{aligned} \mathbf{L}(v_1) &+ RA\mathbf{P}^u(\phi_1, u_{-1}) + RA\mathbf{P}^v(\phi_1, v_{-1}) = 0 \\ \mathbf{L}(v_{-1}) &+ RA\mathbf{P}^u(\phi_{-1}, u_1) + RA\mathbf{P}^v(\phi_{-1}, v_1) = 0 \end{aligned}$$

Equation (42b),

$$\begin{aligned} \mathbf{M}^u(u_1) + \mathbf{M}^v(v_1) &+ RA\mathbf{Q}^u(\phi_1, u_{-1}) + RA\mathbf{Q}^v(\phi_1, v_{-1}) = 0 \\ \mathbf{M}^u(u_{-1}) + \mathbf{M}^v(v_{-1}) &+ RA\mathbf{Q}^u(\phi_{-1}, u_1) + RA\mathbf{Q}^v(\phi_{-1}, v_1) = 0 \end{aligned}$$

We now define the operators in terms of the normal modes variables. For compactness we introduce the following abbreviations,

$$\bar{\gamma}_n = \gamma + in\hat{\alpha}$$
$$\Delta_n = \bar{\gamma}_n^2 - \beta^2$$
$$D_m = \frac{d^2}{dy^2} - m^2\alpha^2$$

Then the operators take the form,

$$\mathbf{L}(v_n) = v_n'''' + [2\Delta_n - R((U_o - c)\bar{\gamma}_n + \sigma)]v_n'' + [\Delta_n^2 - R((U_o - c)\bar{\gamma}_n + \sigma) + RU_o''\bar{\gamma}_n]v_n$$

$$\mathbf{M}^u(u_n) = \Delta_n u_n'' - \Delta_n R[(U_o - c)\bar{\gamma}_n + \sigma]u_n + \Delta_n^2 u_n$$

$$\mathbf{M}^v(v_n) = \bar{\gamma}_n v_n''' + \bar{\gamma}_n[\Delta_n - R((U_o - c)\bar{\gamma}_n + \sigma)]v_n' + R\beta^2 U_o' v_n$$

$$\mathbf{P}^u(\phi_m, u_n) = m^2\alpha^2\phi_m u_n'' + 2im\alpha\phi_m'\bar{\gamma}_n u_n' + im\alpha(D_m\phi_m(2\bar{\gamma}_n + im\alpha) + im\alpha\phi_m\Delta_n)u_n$$

$$\mathbf{P}^v(\phi_m, v_n) = im\alpha\phi_m v_n''' + \phi_m'[im\alpha - \bar{\gamma}_n]v_n'' + im\alpha[(\Delta_n + 2im\alpha\bar{\gamma}_n)\phi_m + D_m\phi_m]v_n' + [D_m\phi_m'(\bar{\gamma}_n + im\alpha) - \phi_m'\bar{\gamma}_n(im\alpha\bar{\gamma}_n + \Delta_n) - im\alpha\phi_m'\beta^2]v_n$$

$$\mathbf{Q}^u(\phi_m, u_n) = im\alpha\phi_m(\Delta_n + im\alpha\bar{\gamma}_n)u_n' - \phi_m'(im\alpha + \bar{\gamma}_n)\Delta_n u_n$$

$$\mathbf{Q}^v(\phi_m, v_n) = im\alpha\phi_m(im\alpha + \bar{\gamma}_n)v_n'' - \phi_m'(im\alpha + \bar{\gamma}_n)\bar{\gamma}_n v_n' + \phi_m''\beta^2 v_n$$

REFERENCES

[1] Herbert, Th., "Modes of secondary instability in plane Poiseuille flow," in: Tatsumi, T. (ed.) *Turbulence and Chaotic Phenomena in Fluids*, Amsterdam: North-Holland, pp. 53-58 (1984).

[2] Herbert, Th., "Analysis of the subharmonic route to transition in boundary layers," AIAA Paper No. 84-0009, 1984.

[3] Herbert, Th., "Secondary instability of plane shear flows - theory and application," in: Kozlov, V. V. (ed.) *Laminar-Turbulent Transition*, Berlin: Springer-Verlag, to appear (1985).

[4] Herbert, Th., "Subharmonic Three-Dimensional Disturbances in Unstable Plane shear flows," AIAA Paper No. 83-1759, 1983.

[5] Herbert, Th., "Three-dimensional phenomena in the transitional flat-plate boundary layer," AIAA Paper No. 85-0489, 1985.

[6] Shubauer G.B. & Skramstad H.K., "Laminar boundary layer oscillations and stability of laminar flow," *J. Aerospace Sci.* **14**, N2, 1947.

[7] Klebanoff P.S., Tidstrom K.D. & Sargent L.M., "The three-dimensional nature of boundary-layer instability," *J. Fluid Mech.* **12**, pp. 1-34, 1962.

[8] Kachanov, Yu. S. & Levchenko, V. Ya., "The resonant interaction of disturbances at laminar-turbulent transition in a boundary layer," *J. Fluid Mech.* **138**, pp. 209-247, 1984.

[9] Saric, W. S. & Thomas, A. S. W., "Experiments on the subharmonic route to transition in boundary layers," in: Tatsumi, T. (ed.) *Turbulence and Chaotic Phenomena in Fluids*, North-Holland, Amsterdam, pp. 117-122 (1984)

[10] Nishioka M., Iida S. & Ichikawa Y., "An experimental investigation of the stability of plane Poiseuille flow," *J. Fluid Mech.* **72**, pp. 731-751, 1975.

[11] Ho C.M. and Huerre P., *Ann. Rev. Fluid Mech.* **16**, pp. 365-424, 1984.

[12] McEwan A.D. & Robinson R.M., "Parametric instability of internal gravity waves," *J. Fluid Mech.* **67**, pp. 667-687, 1975.

[13] Drazin P. and Reid W. **Hydrodynamic Stability**. Cambridge University Press. 1981.

[14] Benney D.J. and Lin C.C., "On the secondary motion induced by oscillations in a shear flow," *J. Phys. Fluids* **3**, pp. 656-657, 1960.

[15] Itoh N., "Three-dimensional growth of finite wave disturbances in plane Poiseuille flow," *Trans. Japan Soc. Aero. Space Sci.* **23**, No 60, 1980.

[16] Craig A.D.D., "Non-linear resonant instability in boundary layers," *J. Fluid Mech.* **50**, pp. 393-413, 1971.

[17] Herbert T. and Morkovin M.V., "Dialogue on bridging some gaps in stability and transition research," in: **Laminar-Turbulent Transition** (ed. Eppler & Fasel), pp. 47-73, Springer-Verlag, 1980.

[18] Maseev L.M., "Occurrence of the three-dimensional perturbations in boundary layers," *Fluid Dyn.* **3**, pp. 23-24, 1968.

[19] Kelly R.E., "On the stability of an inviscid shear layer which is periodic in space and time," *J. Fluid Mech.* **27**, pp. 657-689, 1967.

[20] Pierrehumbert R. T. & Widnall S. E., "The two- and three-dimensional instabilities of a spatially periodic shear layer," *J. Fluid Mech.* **114**, pp. 59-82, 1982.

[21] Nayfeh A.H., "On the non-linear Lamb-Taylor instability," *J. Fluid Mech.* **38**, pp. 619-631, 1969.

[22] Mied R.P., "The occurrence of parametric instabilities in finite-amplitude internal gravity waves," *J. Fluid Mech.* **78**, pp. 763-784, 1976.

[23] Mied R.P., "The instabilities of finite-amplitude barotropic Rossby waves ," *J. Fluid Mech.* **86**, pp. 225-246, 1978.

[24] Drazin P.G., "On the instability of an internal gravity wave," *Proc. R. Soc. Lond. A* **356**, pp. 411-432, 1977.

[25] Nayfeh A.H. and Bozatli A. N., "Secondary instability in boundary-layer flows" *Phys. Fluids* **22**, pp 805-813, 1979.

[26] Orszag S.A. and Patera A.T., "Subcritical transition to turbulence in planar shear flows," in: **Transition to Turbulence** (ed. R.E. Meyer), pp. 127-146, Academic Press, 1981.

[27] Herbert Th. : VPI Report VPI-E-81-35, 1981. See also *Fluid Dyn. Trans.* **11**, pp. 77-126, 1983.

[28] Betchov R. and Criminale W.O. **Stability of Parallel Flows**. Academic, 1960.

[29] Saric W.S. and Nayfeh A.H., "Nonparallel stability of boundary layer flows" *Phys. Fluids* **18**, pp.945-950, 1975.

[30] Squire H.B., "On the stability for three-dimensional disturbances of viscous fluid flow between parallel walls," *Proc. Roy. Soc. London Ser. A* **142**, pp. 621-628, 1933.

[31] Wazzan, A. R., Okamura, T. T. & Smith, A. M. O., "Spatial and temporal stability charts for the Falkner-Skan boundary layer profiles," Douglas Aircraft Co., Report No. DAC-67086, 1968.

[32] Nayfeh A.H. and Mook D.T., **Nonlinear Oscillations**. Wiley, 1979.

[33] Arscott F.M. **Periodic Differential Equations**. Pergamon Press, 1964.

[34] Kleiser L. & Laurien E., "Three-dimensional numerical simulation of laminar-turbulent transition and its control by periodic disturbances," *Second IUTAM Symposium on Laminar-Turbulent Transition, Novosibirsk, 1984*

[35] White F.M. **Viscous Fluid Flow** . McGraw-Hill, 1974.

[36] Herbert, Th., "Subharmonic Three-Dimensional Disturbances in Unstable Plane shear flows," AIAA Paper No. 83-1759, 1983.

[37] Santos G., PhD Thesis, personal communication.

[38] Gottlieb D. and Orszag S.A., **Numerical Analysis of Spectral Methods: Theory and Applications** *Soc. for Ind. and Appl. Math. Phil., Pa, 1977.*

[39] Smith B.T. et al., EISPACK Guide, **Lecture Notes in Computer Science No 6**, Second edition, Springer-Verlag, New York, 1976.

[40] Herbert T., "Secondary instability of plane channel flow to subharmonic three-dimensional disturbances," *Phys. Fluids* **26**, pp. 871-874, 1983.

[41] Saric W.S. , Carter J.D. and Reynolds G.A., "Computation and visualization of unstable-wave streaklines in a boundary layer ," *Bull. Amer. Physic. Soc.* **26**, pp. 1252, 1981.

[42] Kozlov, V. V., "The interconnection of flow separation and stability," in: Kozlov, V. V. (ed.) *Laminar-Turbulent Transition*, Berlin: Springer-Verlag, to appear (1985).

[43] Chandrsuda C., Mehta R.D., Weir A.D. and Bradshaw P., "Effect of free-stream turbulence on large structure in turbulent mixing layers," *J. Fluid Mech.* **85**, pp. 693-704, 1978.

[44] Gaster M., "A note on the relation between temporally increasing and Spatially increasing disturbances in hydrodynamic stability," *J. Fluid Mech.* **14**, pp. 222-224, 1962.

[45] Nayfeh A.H. and Padhye A., "Relation between temporal and spatial stability in three-dimensional flows," AIAA Paper No. 78-1196R, 1978.

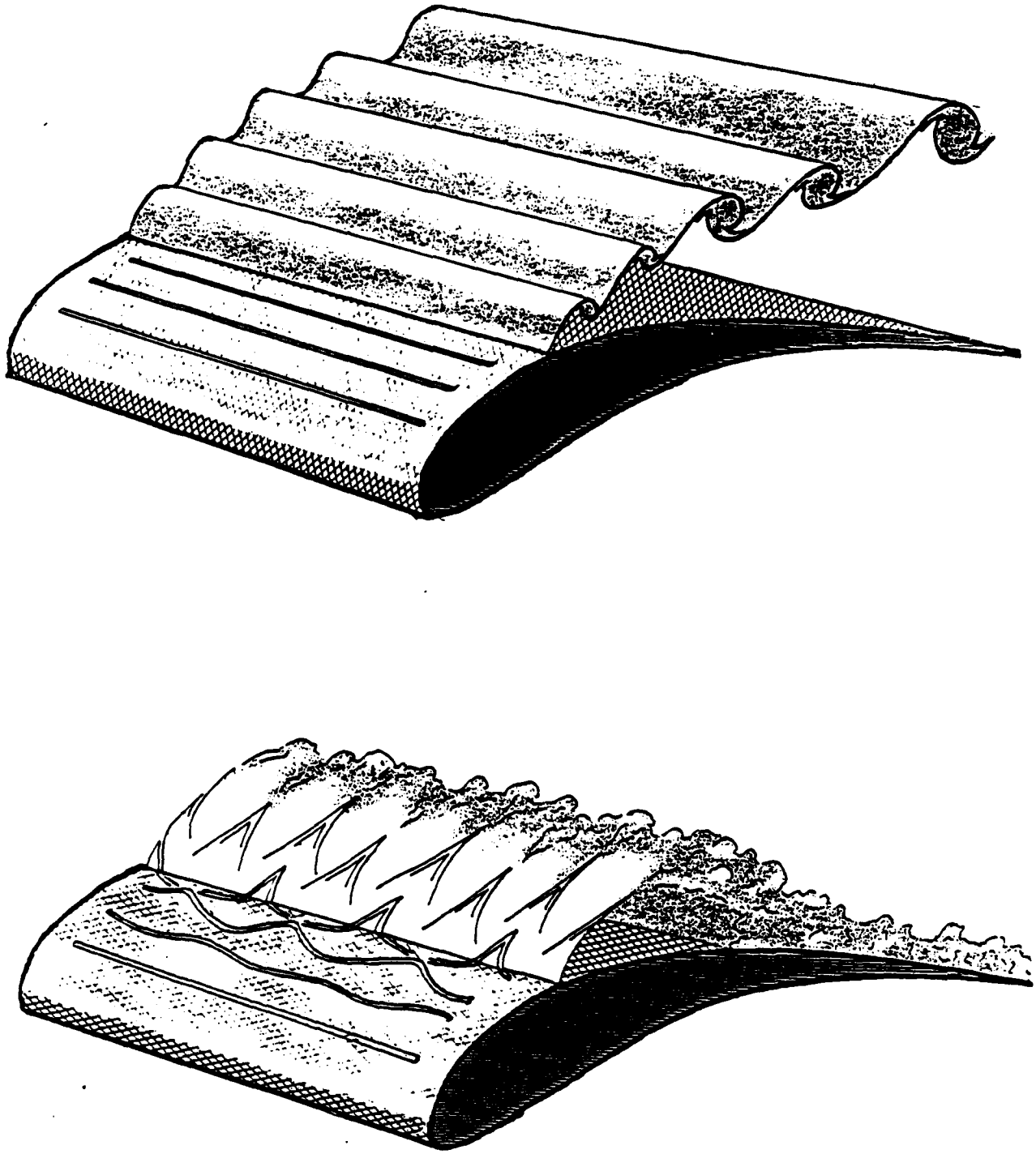

Figure 1. Effect of two-dimensional and three-dimensional disturbances on a separating shear layer. Top, vortex pairing and permanent separation. Bottom, three-dimensional vortex stretching, and breakdown into wall-bound turbulence.

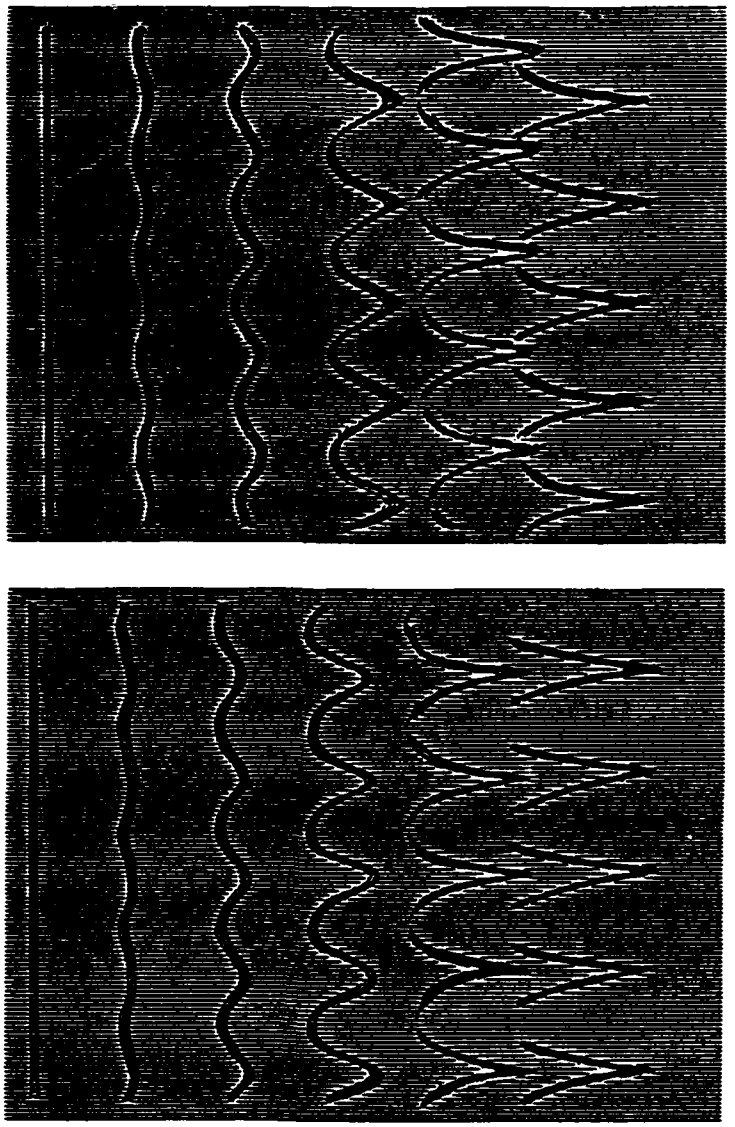

Figure 2 a,b. Streaklines in Blasius boundary layer. The drawings are a reproduction of photos taken by Saric et al. (1983) at the VPI Stability Wind tunnel. Flow is from left to right. Top, subharmonic distuirbance. Bottom, fundamental disturbance.

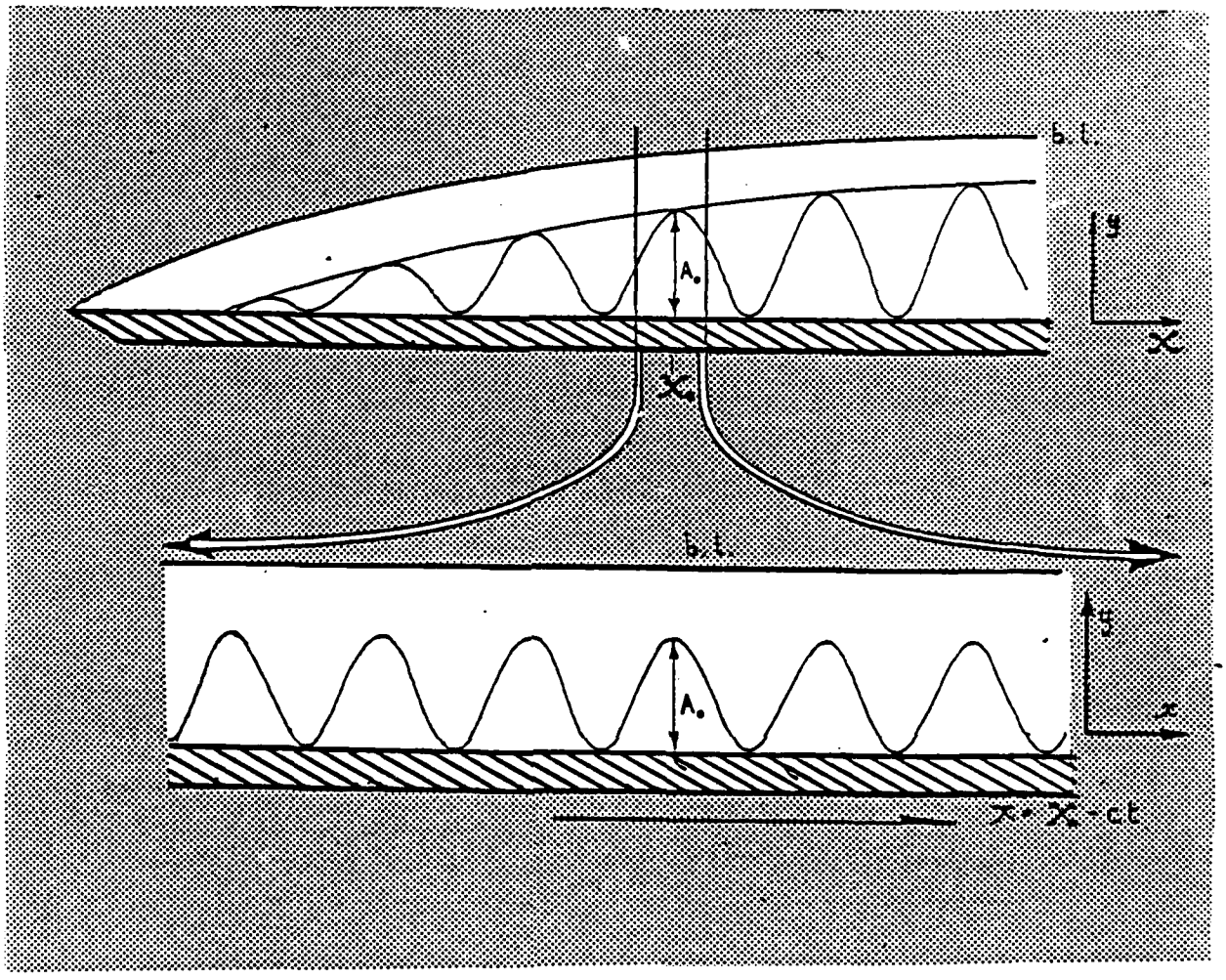

Figure 3. Construction of the periodic basic flow. The weak streamwise variation of boundary-layer thickness and TS wave amplitude are neglected. The local conditions at X_0 are extended into a periodic flow.

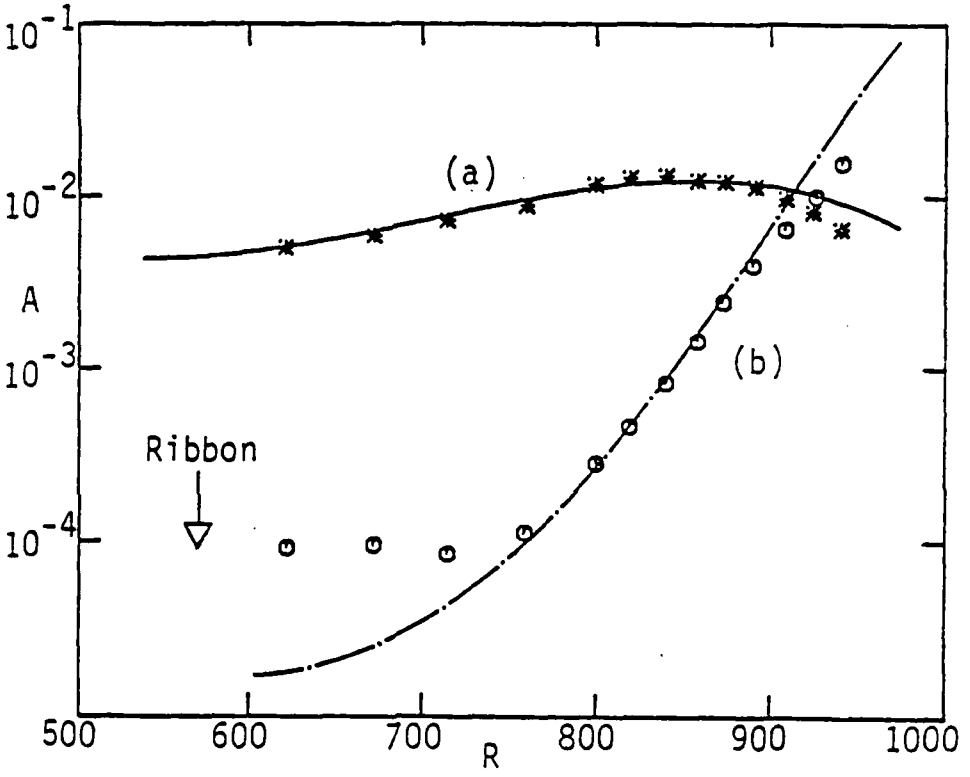

Figure 4. Theoretical and experimental [8] amplitude variation with R for (a) the TS wave ($A_{in} = 0.44\%$) and (b) the subharmonic mode ($B_{in} = 0.00126\%$). $F = 124$, $b = 0.33$, $P = 0$.

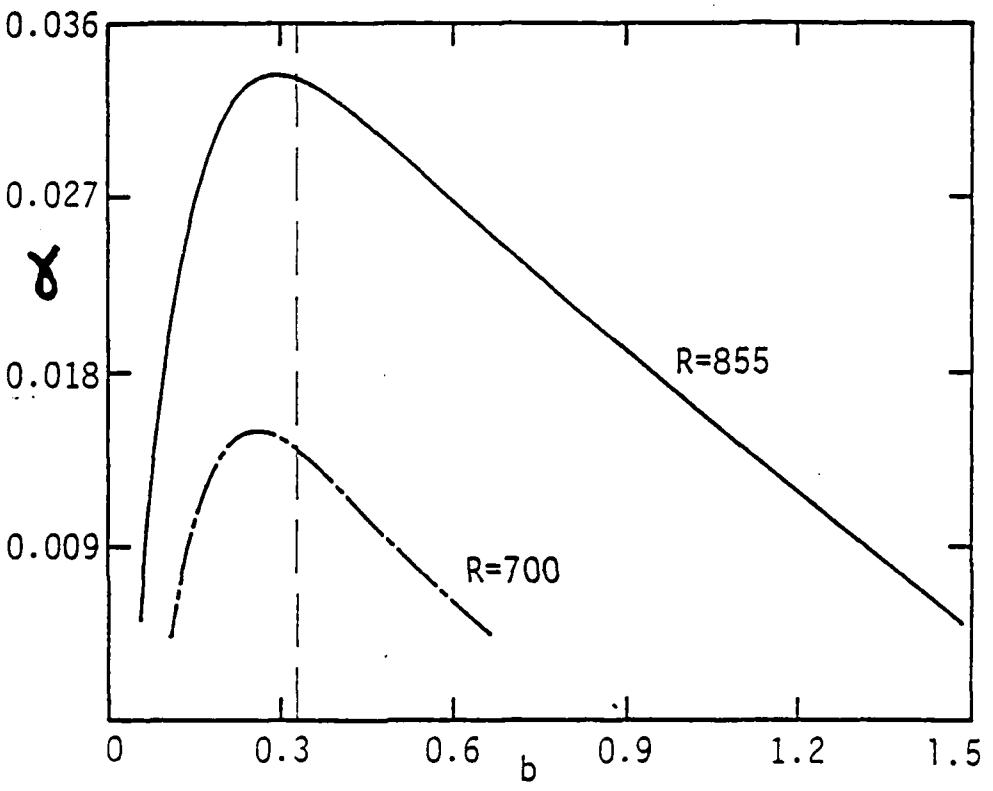

Figure 5. Spatial growth rate γ versus spanwise wavenumber b for the conditions of Fig. 4. The TS amplitudes are $A = 0.74\%$ at $R = 700$, $A = 1.23\%$ at $R = 855$. The vertical line marks the observed wavenumber $b = 0.33$.

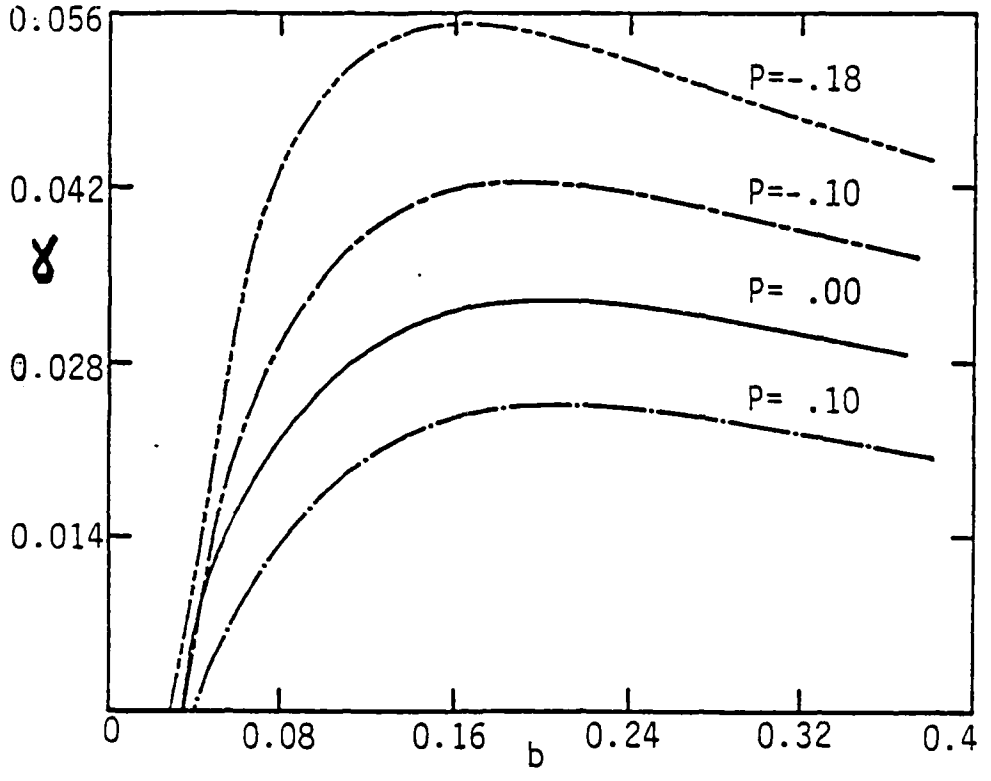

Figure 6. Spatial growth rate γ versus spanwise wavenumber b for various values of the pressure coefficient P. $R = 1168$, $F = 83$, $A = 1\%$.

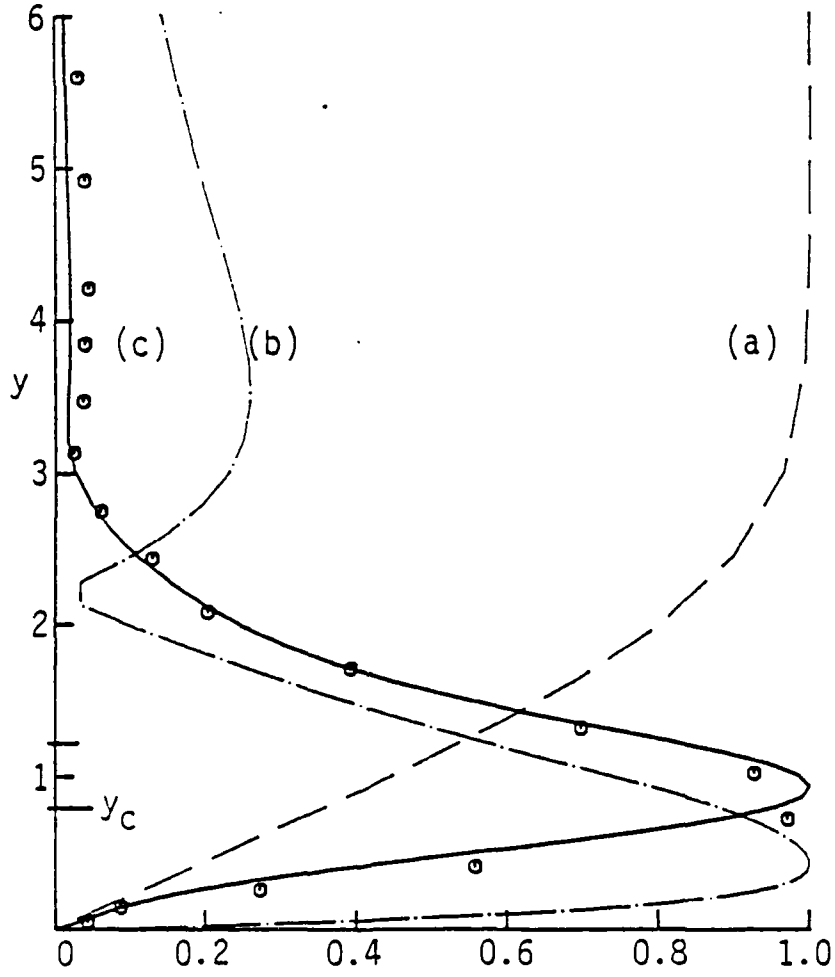

Figure 7. Blasius profile (a), and streamwise rms fluctuations for the TS wave (b) and the subharmonic mode (c) for $R = 873$, $b = 0.33$, $F = 124$, $A = 1.22\%$. Experimental points from [8, Fig 21].

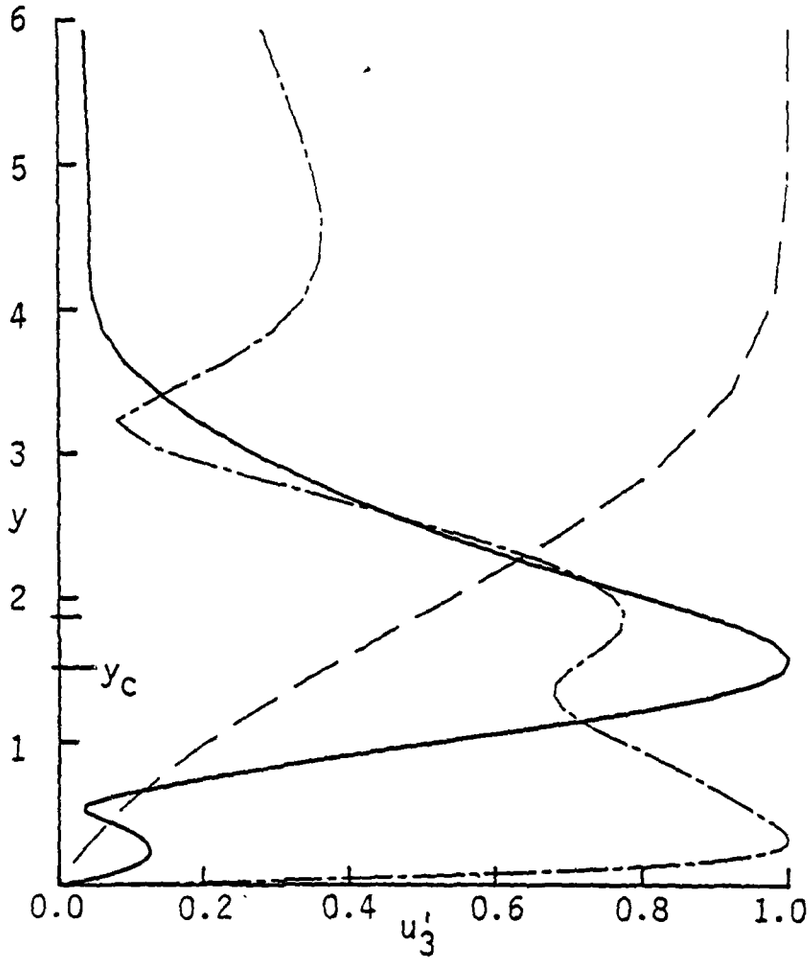

Figure 8. Falkner-Skan profile near separation (a), and streamwise rms fluctuations for the TS wave (b) and the subharmonic mode (c) for $P = -0.18$, $R = 873$, $b = 0.33$, $F = 124$, $A = 1.22\%$.

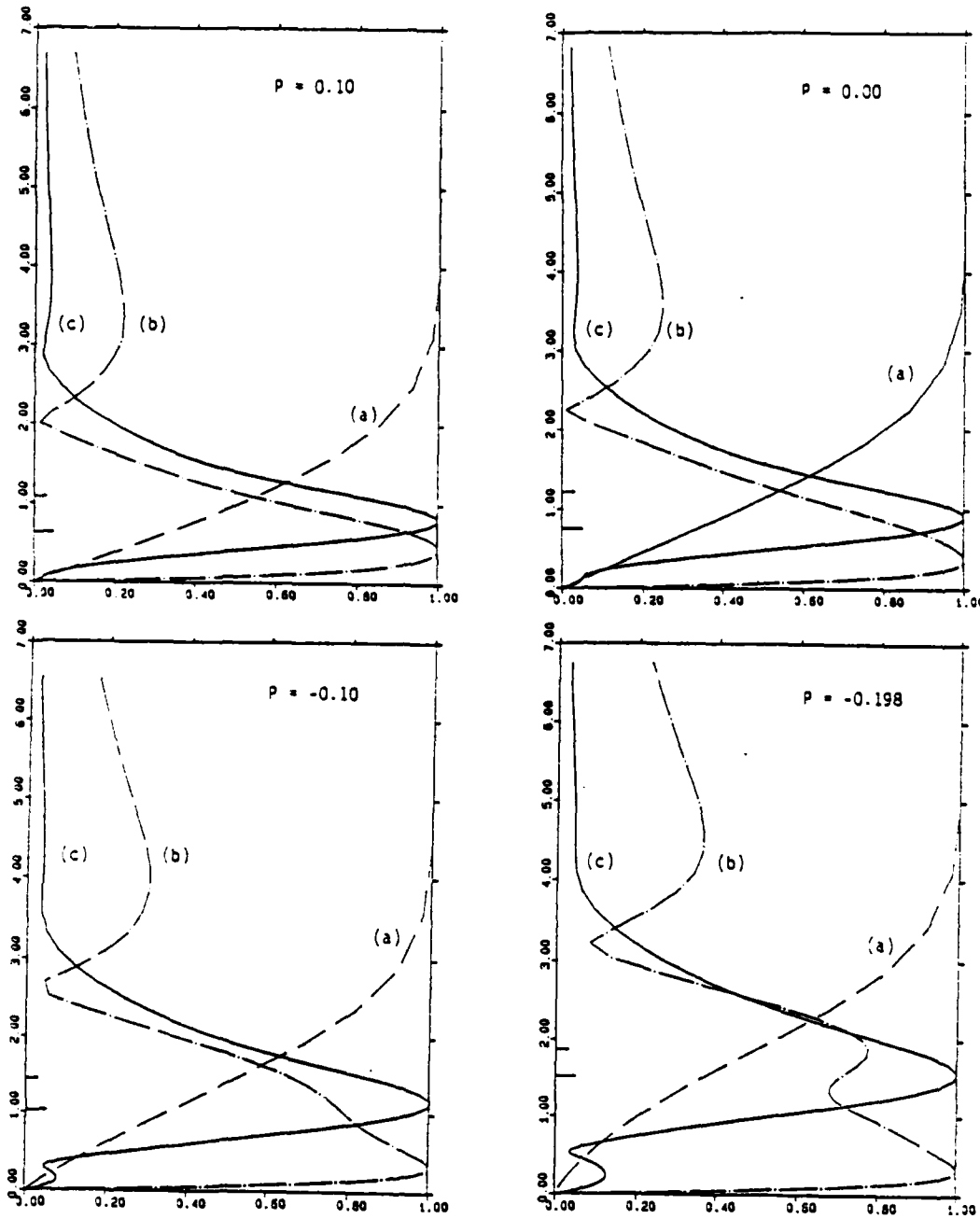

Figure 9. Falkner-Skan profiles (a), and streamwise rms fluctuations for the TS wave (b) and the subharmonic mode (c) for various values of P: Counter-clockwise from top.
$P = 0.10$, $P = 0.00$, $P = -0.10$, $P = -0.18$
$R = 1168$, $b = 0.18$, $F = 83$, $A = 1.00\%$

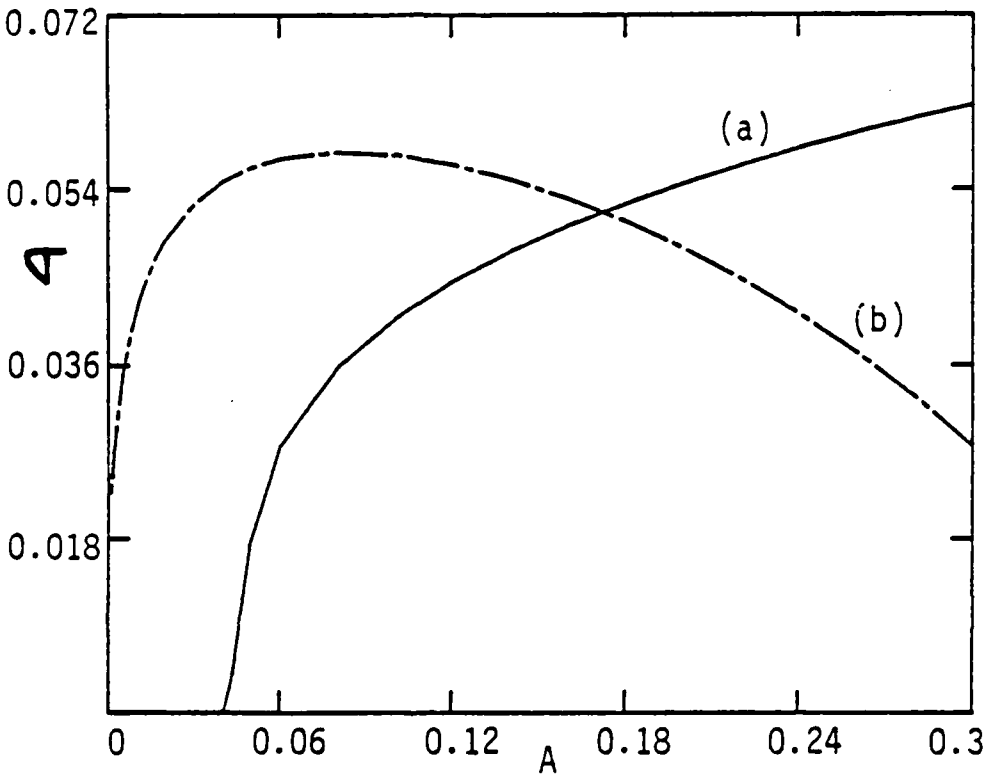

Figure 10. Temporal growth rate σ versus TS amplitude A for tuned modes with $b = 0$ (a) and $b = 0.36$ (b). $P = -.198$, $R = 1000$, $\alpha = 0.5$, $F = 245$.

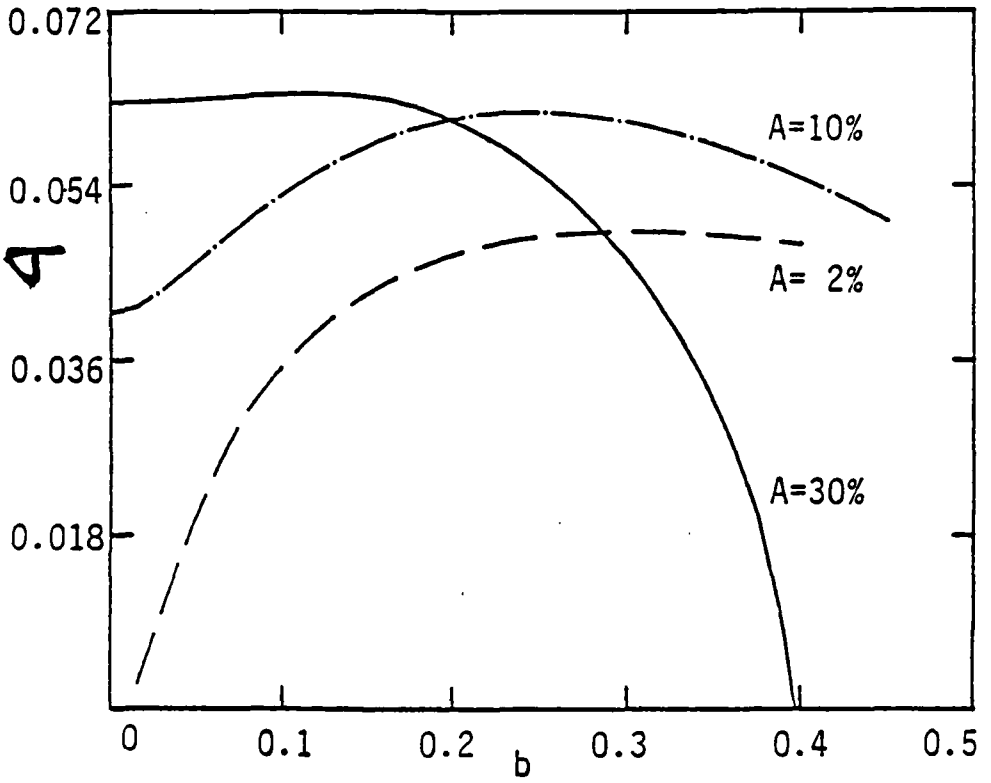

Figure 11. Temporal growth rate σ versus spanwise wavenumber b for various TS amplitudes A in a profile at separation. $P = -.198$, $R = 1000$, $\alpha = 0.5$, $F = 245$.

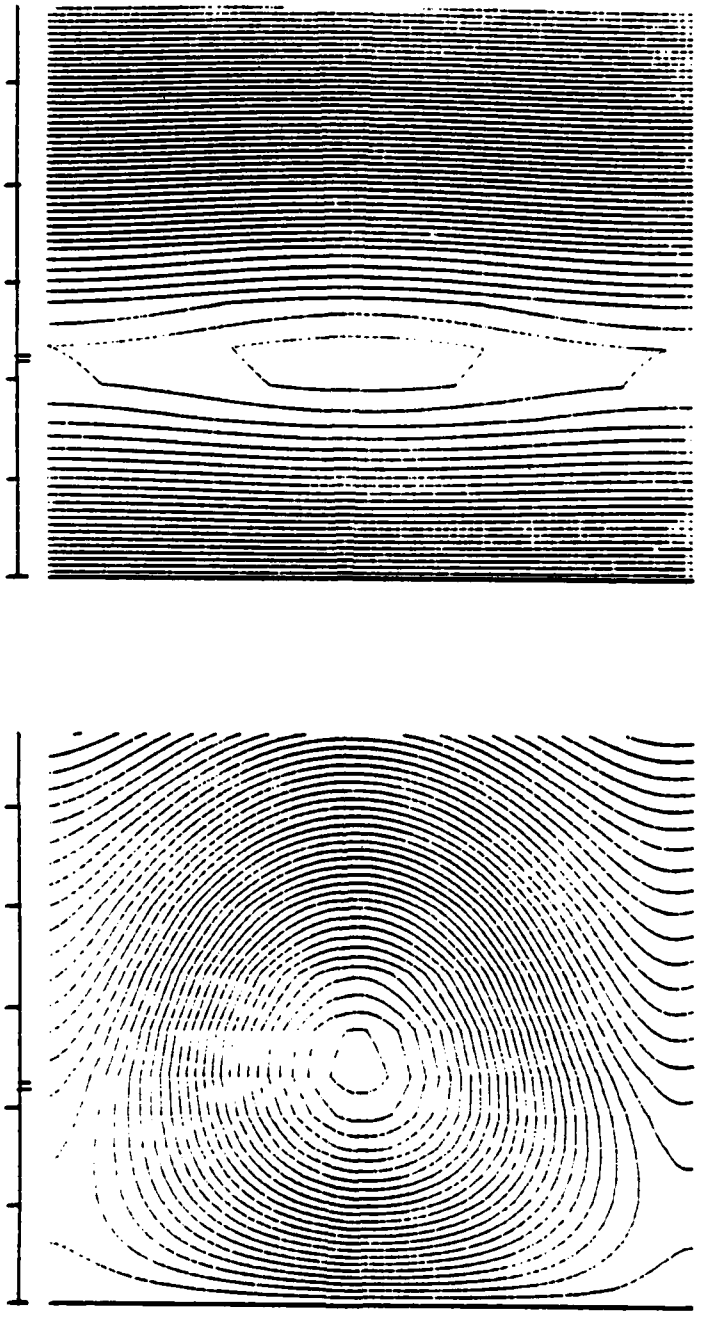

Figure 12. Streamlines in moving coordinate system. Top, $A = 1\%$ bottom $A = 30\%$ $P = -.198$ $R = 1000$ $\alpha = 0.5$

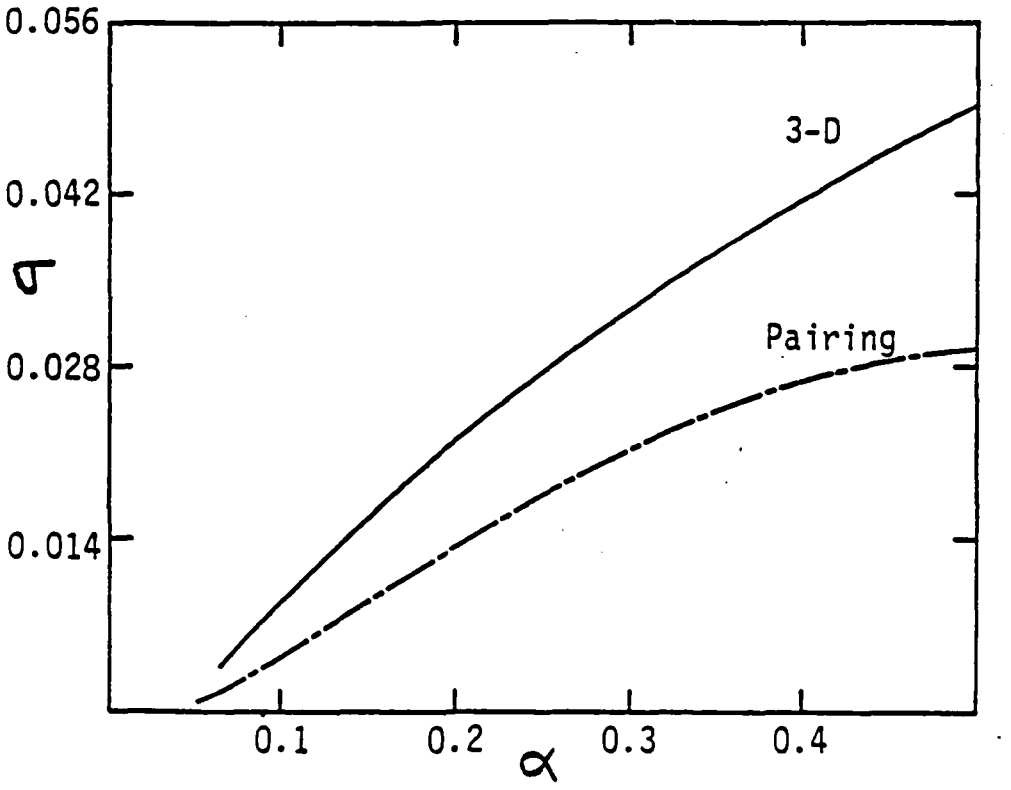

Figure 13. Most unstable tuned mode and detuned vortex pairing as function of α. $P = -0.198$ $R = 1000$ $A = 1\%$

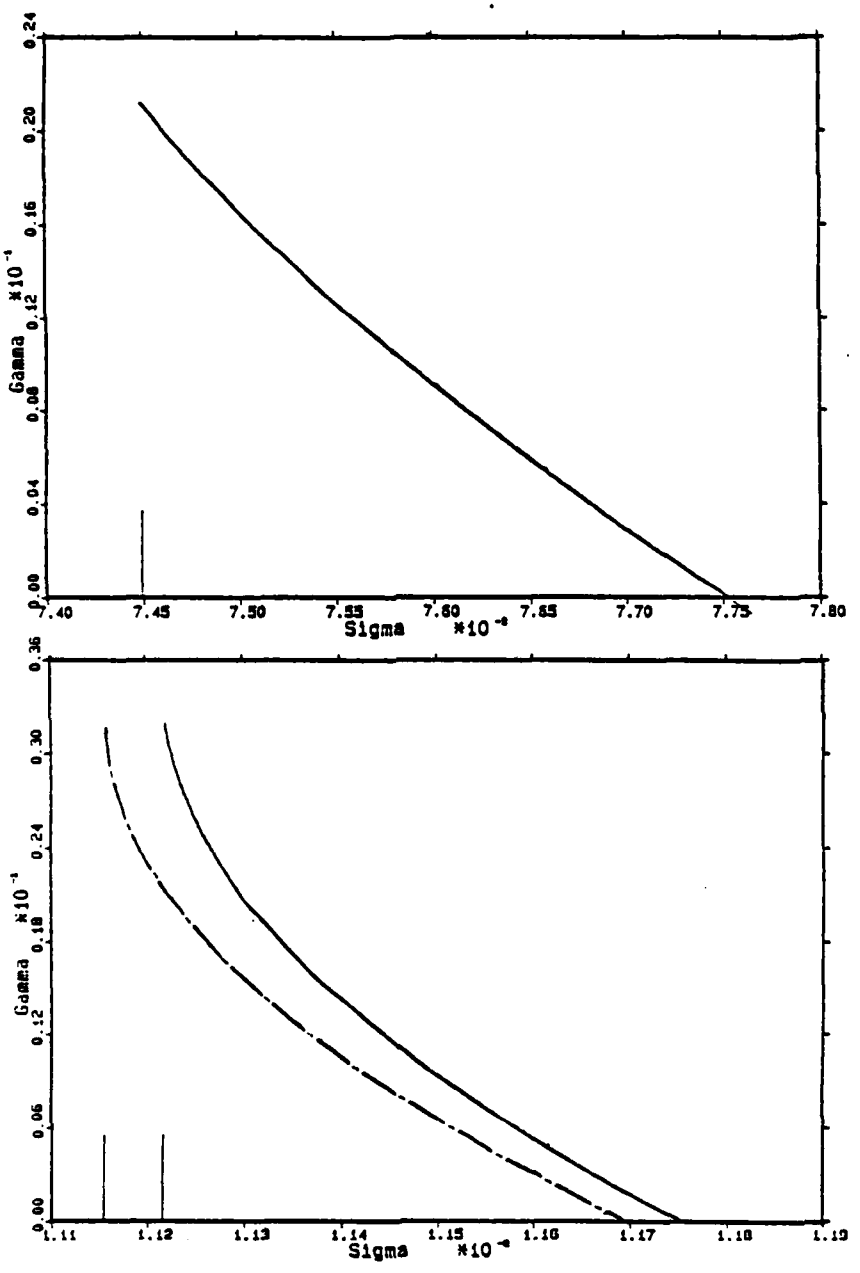

Figure 14. $\gamma = \gamma(\sigma)$ as σ varies from the temporal value to the spatial value (vertical bar). Top, $\beta = 0.09$, close to neutral stability. Bottom, $\beta = 0.18$ and $\beta = 0.32$. Blasius Flow, $R = 1168$, $F = 83$, $A = 1\%$

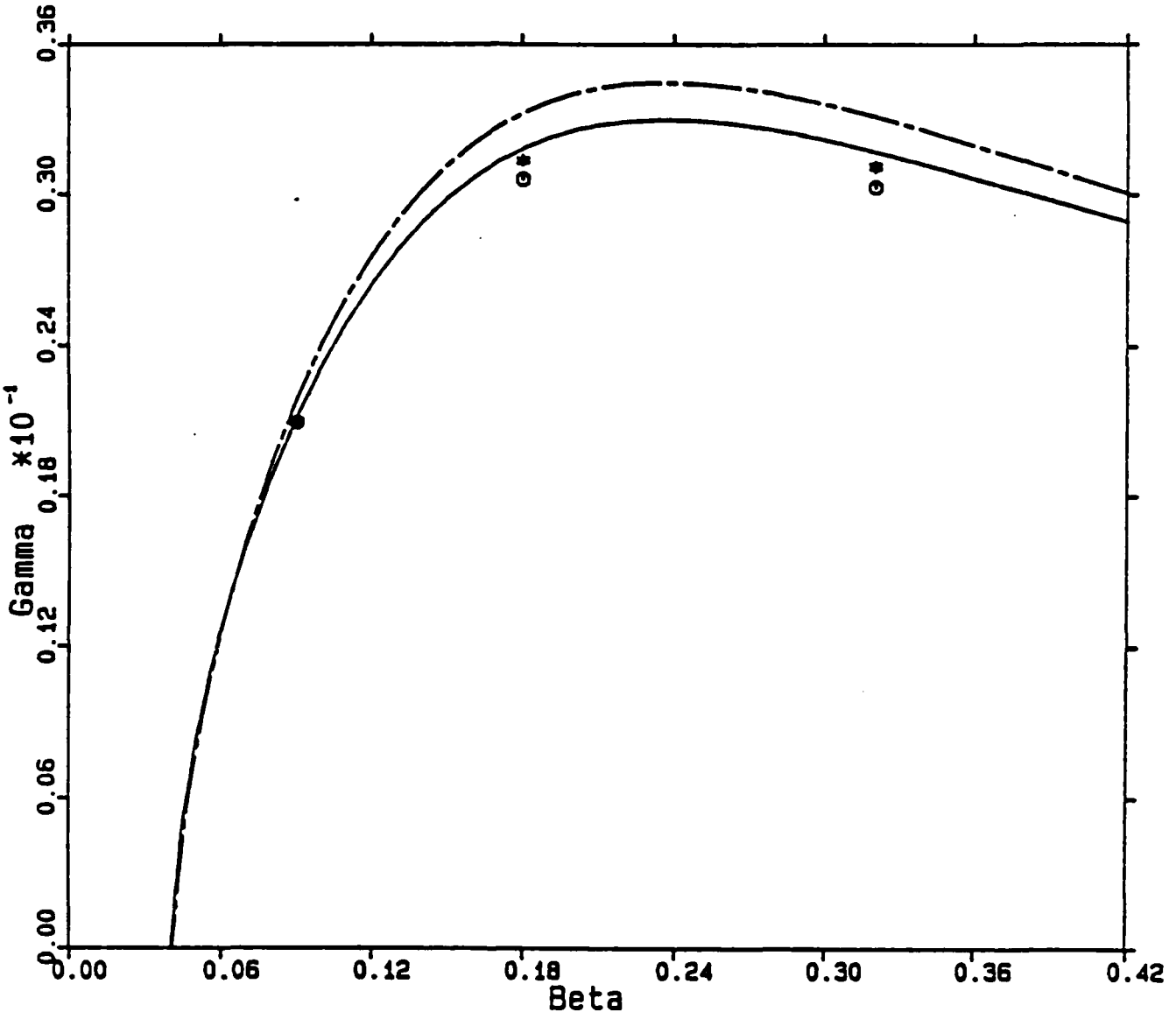

Figure 15. Exact (solid) and transformed ($\gamma = \frac{\sigma}{c}$) spatial growth rates. Blasius Flow, $R = 1168$, $F = 83$, $A = 1\%$
Points * are 2^{nd} order, points θ are 1^{st} order.

VITA

The author was born [redacted], and attended primary and secondary schools in the US, Italy, and Spain. He enrolled in 1979 in the Virginia Tech Enginnering Science and Mechanics curriculum, receiving a Batchlor of Science in 1983. The following September he entered the Graduate School at Virginia Tech on a program of study leading to the degree of Masters of Science in Engineering Science and Mechanics.

TEMPORAL AND SPATIAL GROWTH

OF SUBHARMONIC DISTURBANCES

IN FALKNER-SKAN FLOWS

by

Fabio P. Bertolotti

Committee Chairman: Thorwald Herbert

Engineering Science and Mechanics

(ABSTRACT)

The transition from laminar to turbulent flow in boundary-layers occurs in three stages: onset of two-dimensional TS waves, onset of three-dimensional secondary disturbances of fundamental or subharmonic type, and onset of the turbulent regime. In free flight conditions, subharmonic disturbances are the most amplified.

Recent modeling of the subharmonic disturbance as a parametric instability arising from the presence of a finite amplitude TS wave has given results in quantitative agreement with experiments conducted in a Blasius boundary-layer. The present work extends the analysis to the Falkner-Skan family of profiles, and develops a formulation for spatially growing

disturbances to exactly match the experimental observations.

Results show that subharmonic disturbances in Falkner-Skan flows behave similarly to those in a Blasius flow. The most noticeable effect of the pressure gradient is a decrease (favorable) or an increase (adverse) of the disturbance's growth rate. Due to the lack of experimental data, a comparison of subharmonic growth rates from theory and experiment is limited to the Blasius boundary-layer. A comparison of results from the spatial formulation with those previously obtained from a temporal formulation shows the difference to be small. A connection between disturbance growth in a separating boundary-layer profile and a free shear layer is presented. A modification of Gaster's transformation from temporal to spatial growth rates for secondary disturbances is given.